

A Comprehensive Census of Nearby Infrared Excess Stars

Tara H. Cotten

Department of Physics and Astronomy, University of Georgia, Athens, GA 30602

`tara@physast.uga.edu`

Inseok Song

Department of Physics and Astronomy, University of Georgia, Athens, GA 30602

`song@physast.uga.edu`

ABSTRACT

The conclusion of the WISE mission presents an opportune time to summarize the history of using excess emission in the infrared as a tracer of circumstellar material and exploit all available data for future missions such as JWST. We have compiled a catalog of infrared excess stars from peer-reviewed articles and perform an extensive search for new infrared excess stars by cross-correlating the Tycho-2 and AllWISE catalogs. We define a significance of excess in four spectral type divisions and select stars showing greater than either 3σ or 5σ significance of excess in the mid- and far-infrared. Through procedures including SED fitting and various image analyses, each potential excess source was rigorously vetted to eliminate false-positives. The infrared excess stars from the literature and the new stars found through the Tycho-2 and AllWISE cross-correlation produced nearly 500 ‘Prime’ infrared excess stars and ≥ 1200 ‘Reserved’ stars. The main catalog of infrared excess stars are nearby, bright, and either demonstrate excess in more than one passband or have infrared spectroscopy confirming the infrared excess. This study identifies stars that display a spectral energy distribution suggestive of a secondary or post-protoplanetary generation of dust and they are ideal targets for future optical and infrared imaging observations. The final catalogs of stars summarizes the past work using infrared excess to detect dust disks and with the most extensive compilation of infrared excess stars (~ 1750) to date, we investigate various relationships among stellar and disk parameters.

Subject headings: infrared excess, circumstellar material: general, debris disks, stars

1. Introduction

Excess emission in the infrared (IR excess, hereafter) provides a useful tracer of the dust in a circumstellar disk due to the process by which the dust grains are heated by the starlight and reemit at longer wavelengths. Identifying each distinct evolutionary phase can be challenging but possible since the shape of the IR excess depends on the size, temperature, and composition of the emitting dust grains. While it is understood that as the protoplanetary disk evolves, the gas and dust is cleared from the inner region closest to the star and then from the outer regions (Wyatt et al.

2015), the discovery of the first debris disk around Vega (Aumann et al. 1984) using the *InfraRed Astronomical Satellite* (IRAS; Beichman et al. 1988), provided evidence for a secondary generation of dust. The secondary origin of this dust around a mature stellar system must be the result of the collisional grinding of planetesimals, comets, and asteroids (Kenyon & Bromley 2008). The information gathered from IR excess stars provides a link to the formation and evolution of exoplanets (Wyatt 2008).

Many studies (Beichman et al. 2006b, Bryden et al. 2006a, Su et al. 2006, Gautier et al. 2007, Moro-

Martin et al. 2007, Rhee et al. 2007, Hillenbrand et al. 2008, Trilling et al. 2008, Carpenter et al. 2009, Greaves et al. 2009, Morales et al. 2012, Bulger et al. 2013, Eiroa et al. 2013, Patel et al. 2014) have confirmed the use of excess emission in the infrared as an indicator for circumstellar dust. Table 1 shows the notable infrared surveys that were developed to improve the sensitivity of IRAS and were used in the detection of debris disk stars. Circumstellar material in locations analogous to our Kuiper and Asteroid belts can be detected by excess emission at $\geq 10\mu\text{m}$ wavelengths and the past few decades has allowed for the exploration of disk properties such as dust temperature ranging from very cold (~ 10 K) to warm (~ 500 K). At the current time, all major mid- to far- infrared space missions have finished operations, including the most recent *Herschel Space Observatory* (Pilbratt et al. 2010) and the *Wide-Field Infrared Survey Explorer* (WISE; Wright et al. 2010). Studies have shifted to analyze data available through archives. With the advent of new infrared missions still a couple years in the future (e.g. *James Webb Space Telescope*, *JWST*; Gardner et al. 2006), we are at a unique time in which we can devote adequate effort to thoroughly characterize known IR excess stars in the solar neighborhood.

The use of IR excess has generated hundreds of publications as well as thousands of claimed IR excess stars. Focusing specifically on sources that attest to dust undergoing recent collisional activity, as in the case of debris disks, each of these studies presented various source selection and infrared excess criteria. However, many problematic IR excess candidate stars present conflicting evidence based on these different criteria. Therefore, a vetted list of IR excess stars is needed to maximize the scientific return of imminent next generation missions (*JWST* and *WFIRST*; *Wide-Field InfraRed Survey Telescope*) and currently ongoing missions with new extreme adaptive optics instruments such as *GPI* (*Gemini Planet Imager*, Macintosh et al. 2006) and *SPHERE* (*Spectro-Polarimetric High-contrast Exoplanet REsearch*, Beuzit et al. 2008). Yet, we need to unify the search for IR excess stars through simultaneous examination of both previous and new findings of IR excess.

The most comprehensive catalog of nearby IR excess stars is created here through the combi-

nation of 1) a literature search for mostly far-IR excess stars discovered with the *Spitzer Space Telescope*, *Herschel Space Observatory*, and IRAS (Section 2) and 2) a new search for mid-IR excess stars using the all-sky *Wide-Field Infrared Survey Explorer* catalog (AllWISE, Wright et al. 2010; Section 3). The paper begins with a description of our literature search of over 200 published articles that present many IR excess and debris disk stars and we describe our reanalysis of the claimed IR excess. Section 3 recounts our new investigation into IR excess stars with warm dust radiating at $\geq 10\mu\text{m}$ through the cross-correlation between the Tycho-2 catalog (Høg et al. 2000) and the AllWISE catalog, providing significant additions to historical infrared studies. We compare our Tycho-2/AllWISE cross-match to similar warm dust studies performed recently in Section 4. Characteristics of the final IR excess catalog is provided in Sections 5 and 6, followed by our conclusions and future work described in Section 7.

2. Literature Search

Following Aumann et al. (1984), many studies reported new discoveries of IR excess stars. To summarize known IR excess stars from the literature, we select a few pivotal investigations involving IRAS and *Spitzer* as well as a review article: Rieke et al. (2005), Rhee et al. (2007), and Wyatt (2008). Besides the lists of authentic excess stars in each of these reports, citations included in these articles provide the basis of our literature search. We meticulously comb over 230 articles (displayed in Table 2) that cite at least one of these three pivotal papers for stars claimed to have IR excess and compile a database of these objects. The collection of previous publications excludes any searches for IR excess candidates that singularly used the *Wide-Field Infrared Survey Explorer* (WISE), since this was the intent of our new infrared search presented later in Section 3.

In our creation of the main IR excess star catalog, we focus on identifying nearby, main sequence stars with post-protoplanetary disks. However, without available age information, we select disks through a characteristic inspection of the shape of the spectral energy distribution. We assume that stars having photospheric AllWISE fluxes at W1

($3.5\mu\text{m}$) and W2 ($4.6\mu\text{m}$) bands with clear excess emission at mid- to far-IR are sources involved in secondary dust generation. We reserve a discussion of the ages of these systems for a forthcoming paper using optical spectroscopy to characterize our primary target IR excess stars. Using these criteria, it is reasonable to assume that we will be missing the youngest disk counterparts including many T Tauri and Herbig Ae/Be disks. Furthermore, we avoid publications that sought to find circumstellar disks around very distant stars (> 500 pc; e.g. Cloutier et al. 2014) or white dwarfs (e.g. Barber et al. 2012). For example, we keep only stars from Luhman & Mamajek (2012) that can be matched best to an ‘older’, inner cleared disk with no excess emission at W1 or W2. Moreover, some studies provide lists of rejected sources (Rhee et al. 2007, Ballering et al. 2013) that enabled us to avoid stars confirmed to be non-excess.

To investigate the nature of apparent IR excess emission, we create a spectral energy distribution (SED) of all compiled candidate IR excess stars and perform several procedures to reduce including any false-positives. The SED displays flux density versus wavelength from measured photometry which is then fit to a Phoenix NextGen main sequence stellar model (Hauschildt et al. 1999). For more details regarding the SED models and fitting, refer to Rhee et al. (2007). Roughly 820 stars were compiled and assessed from the literature search. However, since previous publications include evolved stars whose IR excess mechanism is different from that of main sequence stars, we checked all IR excess candidate stars using SIMBAD and remove 20 stars with luminosity classes of I, II or III. Lastly, two key procedures for eliminating false-positive excess stars include the visual inspection of the SED and AllWISE images to remove possible contaminated sources (explained in full detail in Section 3.2.6). We use the VizieR database to gather additional photometry from optical to far-IR wavelengths if available. The multitude of photometric measurements ensures a reliable SED fit to the stellar photosphere and enables us to quantify the number of passbands which display IR excess (`‘Num.Excess’`). Section 3.2.7 has more details regarding the parameter `‘Num.Excess’`. We remove 65 stars having photospheric flux at far-IR wavelengths (i.e. showing no IR excess).

Among IR excess publications, Chen et al. (2014) is notable because they provided Spitzer IRS spectra of over 300 stars. When available, they also reported MIPS 24 and $70\mu\text{m}$ measurements. Because the evidence of excess determined from infrared spectroscopy aids in the reliability of IR excess from photometry alone, we retain most stars from Chen et al. (2014) unless the IRS spectra is consistent with the photosphere.

To create the most useful catalog of IR excess stars for more efficient future follow-up observations, we implement additional restrictions for a star to be included in the “Prime” table: (1) AllWISE W3 ($12\mu\text{m}$) or W4 ($22\mu\text{m}$) flux being greater than 10 mJy, (2) distance within 120 pc and (3) either multiple passbands demonstrating IR excess (`‘Num.Excess’`>1) or 1 passband of IR excess and IRS spectroscopic confirmation of the photometric excess. These requirements ensure that stars in our final catalog are bright enough to be fully characterized. The distance restriction is sometimes relaxed to include few interesting stars with corroborating IRS spectra, however, no star beyond 150 pc was included. Our choice of distance cut, 120 pc, is mainly to remain inside of the local bubble so that we can ignore interstellar reddening and nearby star-forming regions.

After all removals and restrictions, the literature sample of “Prime” IR excess stars (Table 3) contains ~ 430 unique targets. Distant, faint, and marginal excess candidates are maintained in our “Reserved” star catalog (Table 4, an additional ~ 300 stars). Hereafter, we shall refer to this list as the “literature IR excess stars”. The catalog of literature IR excess stars and information regarding the star and disk parameters for this sample of stars is included in Tables 3 and 4. Each table’s details are explained fully in Section 3.2.7.

3. Tycho-2 & AllWISE

3.1. Total Proper Motion and Cross-Correlation

Analysis of photometric excess based on stellar SEDs requires precise optical photometry in order to constrain the spectral shape (i.e., the stellar effective temperature). Thus, we cross-correlate a large optical survey (the Tycho-2 Catalog of the 2.5 Million Brightest Stars as released in 2000; Høg et al. 2000) and the most comprehensive all-

sky mid-infrared survey (the AllWISE all-sky catalog; Cutri et al. 2013) to create a massive list of sources. Lacking accurate parallax measurements for most Tycho-2 stars, we implement a restriction on the proper motion magnitude defined by:

$$\mu_{total} = \sqrt{(\mu_{\alpha})^2 + (\mu_{\delta})^2} \geq 25.0 \text{ (mas/yr)}, \quad (1)$$

as a proxy for distance corresponding to stars within 200 pc. The stars within 100 pc that also have total proper motions greater than 25 mas/yr recovers 91%. The proper motion criterion solely applied to the Tycho-2 catalog assembles 515,518 stars.

We perform a cross-match of the proper motion selected Tycho-2 sample and the AllWISE survey comparing the catalog positions. Considering the twenty year baseline between these two catalogs implies an object with a large proper motion ($\gtrsim 0.1''/\text{yr}$) would be displaced by $2.0''$, however, we execute a proper motion correction to Tycho-2 positions using the Tycho-2 proper motions in order to mitigate this effect. We select sources with a $5.0''$ match radius between AllWISE and Tycho-2 sources and the cross-match returns 99.6% of the Tycho-2 sample. The cross-correlated sample contains 513,478 objects.

3.2. IR Excess Selection Procedures

This section provides our algorithm to reduce the starting sample from over 500,000 stars to a reliable sample of main-sequence, IR excess candidate stars. A number of criteria are used to remove evolved stars, poor photometric quality data, and false positives. A summary of the procedure can be found in the flowchart shown in Figure 1.

3.2.1. Giants

A non-negligible fraction of the cross-correlated sample will inherently be evolved stars that are not discernible from main sequence stars. Although there are some interesting exceptions of giants with IR excess (i.e. Phoenix giants, see Melis et al. 2009), we will focus only on main sequence stars where IR excess points to circumstellar material suggestive of planetary relevance.

To gain insight into the contamination fraction of giant stars in our sample, we cross-match our

sample of 513,478 Tycho-2/AllWISE sources with the *Hipparcos* catalog (van Leeuwen 2007). A $5.0''$ search radius ensures the closest match with the *Hipparcos* catalog and returns 54,016 stars with measured parallax. A similar color-magnitude diagram (CMD) method of excluding evolved stars using the *Hipparcos* catalog was performed by Rhee et al. (2007) and more recently by Patel et al. (2014). We convert the Tycho-2 B_T and V_T magnitudes to the Johnson system using correction factors (Bessell 2000). We choose (V-W2) for the color of our CMD since our sources have AllWISE data and this color provides the longest, useful color baseline. Figure 2 displays (V-W2) color versus the absolute visual magnitude for the 54,016 Tycho-2/AllWISE/*Hipparcos* sources and the well-structured evolutionary separations between the white dwarfs, main sequence, and giant branch stars. Our choice of excluding giants and white dwarfs is shown by the dashed red lines and blue ‘X’s in Figure 2 defined by:

$$(V - W2) > 2.0 \text{ and } M_V \leq 5.0 \quad (2)$$

$$M_V \geq 2.5 \times (V - W2) + 1.8. \quad (3)$$

This procedure identifies 15,071 stars as giants and 581 white dwarf stars among 54,016 Tycho-2/AllWISE/*Hipparcos* stars. The fraction of evolved stars from a sample of about 54,000 is about 30% and we expect this same contamination rate of the Tycho-2/AllWISE sample that lack *Hipparcos* data. We anticipate the majority of remaining giant stars to belong to K and M spectral types since early type giants are rare due to their short lifetimes.

Since the CMD method requires *Hipparcos* data, we also investigate a method to remove evolved stars based on various color-color diagrams. Bessell & Brett (1988) demonstrated using color-color diagrams to identify the divergence of late-type main sequence and giant tracks that appear to diverge at approximately early M type. For our study, we want to identify colors which are able to distinguish G and K type dwarfs from giants. We compare dwarf and giant model fluxes at various passbands to determine a useful color which bifurcates the evolved branch at spectral types earlier than M. We find that the broadband colors of H - W2 versus V - J shows this distinction most clearly (Figure 3). We define the conservative polynomial to remove objects falling within

the red dashed curves:

$$y = 0.05x^3 - 0.19x^2 + 0.23x + 0.13 \quad (4)$$

where $x = (V-J)$ and $y = (H-W2)$. The selection using the dashed lines removes 77% of the known *Hipparcos* giant sample and 82% of the literature giant sample. Using the V-J and H-W2 color-color cut, it demonstrates that about 80% of known giants can be flagged while only about 2% of main sequence stars are lost. So, by applying this color-color cut in combination with the expected contamination rate from the CMD, we expect that only $\sim 6\%$ of the final Tycho-2/AllWISE sample will be giants.

3.2.2. AllWISE Photometry

We compare the profile-fit and aperture derived photometry as an additional analysis of the reliability of the AllWISE photometric measurements. While the AllWISE explanatory supplement recommends using the profile-fit photometry to avoid the poor aperture photometry at the saturation limits ($W1 > 8.0$, $W2 > 7.0$, $W3 > 3.8$; Cutri et al. 2013), we believe that unsaturated, well-behaving stars should have similar photometry derived from both methods. We remove sources for which this is not the case by fitting a standard Gaussian to the differences between the aperture and profile-fit magnitudes at each AllWISE passband and exclude stars having differences in photometry outside of 2.5σ . Nearly 6000 stars had photometry that we would term unreliable. These sources tend to be contaminated by nearby ($\lesssim 12''$) brighter objects such as stars, galaxies, or nebulae or cases of strong cirrus contamination in either W3 or W4. The number of stars in our sample after removing the giants and poor photometry sources is 245,924.

For accurate SED fitting, we remove over two thousand stars without a complete set of measurements from Tycho-2, 2MASS, and AllWISE. Some of the stars in our final sample may have poorer quality data according to the flags from the individual catalogs. However, we continue to use this data rather than disregard those magnitudes as it improves the SED fitting. The only instance that photometric measurements do not improve the SED fit are upper limits and so we have eliminated stars with upper limits at these crucial wavelengths.

3.2.3. SED Fitting

In our SED fitting, NextGen (PHOENIX code version 9.1, Hauschildt et al. 1999) and Kurucz model atmospheres are fit against observed photometric measurements. Between two models, there is a systematic difference of about ~ 120 K in the best fit stellar temperature. Because of the small difference between two models and to avoid mixing two models in our analysis, we decide to use only the NextGen models in our SED fitting. The SED fitting algorithm converts all the photometric measurements into flux and compares them to the grid of available temperatures and selects the best agreement between model and data using a χ^2 minimization technique (Refer to Rhee et al. 2007 for complete details). After producing a good fit to the photosphere, the mid-infrared Rayleigh-Jeans tail provides a comparison for excess emission above the photosphere.

3.2.4. Spurious AllWISE Saturation Correction

Upon inspecting a number of SED fits using the procedure described in Section 3.2.3, we noticed an issue of overestimated fluxes in AllWISE measurements. Sources brighter than 8.1, 6.7, 3.8, and -0.4 mag at W1 through W4, respectively, are saturated and thus, the fluxes are overestimated (Cutri et al. 2013). Patel et al. (2014) presents a similar discussion but a different analysis. The WISE team described this bias for $W2 < 6.5$ mag and illustrated this finding through their Figure 8 in Section VI.3.c.4 of Cutri et al. (2012), however, at the time of writing they did not offer a solution to the nearly 0.5 mag over-estimate for the brightest objects. The bright candidates in our sample demonstrate this spurious flux mainly at W2. Since this effect is not intrinsic to the object, we develop a correction to the AllWISE W2 flux using over 26,000 early A and F stars ($T_{*,SED} \geq 6000$ K) selected by their best fit stellar temperature from the SED. These earlier type stars have a smooth Rayleigh-Jeans tail at every AllWISE passband while later type stars develop strong carbon monoxide (CO) absorption features near W2 ($4.6 \mu\text{m}$). Figure 4 displays the over-estimation of the flux density specifically for magnitudes brighter than 7 in W2. The correction function involves a series of logarithms as described below:

W2 ≤ 7.0 mag:

$$y = 3.28 - 168.55 \log(x+0.084)^{-1} + 164.78 \log(x+0.003)^{-1} \quad (5)$$

where the value of y refers to the difference between the measured and predicted W2 flux in Jansky and the value of x refers to the AllWISE catalog magnitude.

3.2.5. Qualification of Excess

Our infrared excess qualifications use the predicted flux values at the AllWISE passbands determined by the best fit SED after applying the saturation correction. We define the amount of IR excess in terms of a ‘Significance of Excess’ as:

$$\text{Significance of Excess} \equiv \frac{F_{AllWISE} - F_{predicted}}{\sqrt{(\sigma_{AllWISE}^2 + \sigma_{cal}^2)}} \quad (6)$$

where $F_{AllWISE}$ is the measured flux at a given AllWISE passband and $\sigma_{AllWISE}$ is the uncertainty in that measurement combined with an absolute calibration uncertainty (σ_{cal}) defined by Jarrett et al. (2011) and Cruz-Saenz de Miera et al. (2014) to be 4.5% in W3 and 5.7% in W4. The calibration uncertainty was derived by Jarrett et al. (2011) through comparison of AllWISE photometry and *Spitzer* data for a set of standard stars. $F_{predicted}$ represents the photospheric flux value from the SED fit predicted at each AllWISE passband. As mentioned previously, we expect W1 and W2 to be consistent with the stellar photosphere and use W3 and W4 excess for our final IR excess candidates. In our analysis, we do not include a color correction of AllWISE measurements because the effects are small.

Figure 5 displays the significance of excess versus stellar temperature for the 243,354 stars in our sample. The figure shows a significant decreasing trend in the significance of excess with decreasing stellar temperature, in particular, for stars with $T_{*,SED} < 4000$ K. AllWISE W3 shows a steeper decline and we believe this is inherently due to the larger passband of W3 than W4. Wright et al. (2010) mentions a color correction applied to the flux in W3 would be larger than for any other

passband and is exacerbated by the variability and activity found around nearby late-type stars. Further, Wright et al. (2010) describes the in-flight discrepancy found between red and blue sources that implies that the coolest stars will have a W3 flux that is measured to be fainter than models (i.e. a negative significance of excess). To remove this effect, we fit a curve to this trend for stars with temperature less than 4000K. The functional form of the curve for the W3 and W4 significance of excess (SOE) correction is:

$$W3 : SOE = -2.9 \times 10^{-6} \times T_*^2 + 0.03 \times T_* - 62.22 \quad (7)$$

$$W4 : SOE = -1.7 \times 10^{-6} \times T_*^2 + 0.02 \times T_* - 37.92 \quad (8)$$

where T_* refers the the best fit stellar temperature from the SED. The stars in the other temperature regions do not show any significant trend requiring a correction.

After applying the correction to the stars with the coolest temperatures ($T_{*,SED} < 4000$ K), histograms of the significance of excess are displayed in Figure 6 for each temperature division for W3 and W4. Our selection of significant IR excess uses a Gaussian fit to each apparent population of non-excess stars shown by the red dashed curve. The mode of the significance of excess is offset from zero in the positive direction in many histograms, likely due to a combination of model uncertainties, Malmquist bias, and other unknown uncertainties. We initially select the best excess candidates using the Gaussian fits and retain stars beyond the solid, vertical, black lines representing 5σ in W3 or W4 for each temperature division, however, recognizing that many past studies (Vican & Schneider 2014, Patel et al. 2014) isolated cases of marginal W4 excess which may in fact prove to be true detections of IR excess, we also include the sample of stars with W3 or W4 greater than 3σ shown by the vertical dashed line in Figure 6. This procedure identifies nearly 4300 stars with significant IR excess.

3.2.6. Contamination Inspection

Given the likelihood that many false-positive stars are due to source confusion in AllWISE images due to a large mid-IR beam size, a series of quantitative image analyses are presented.

These sources of contamination include cirrus or foreground infrared sources, adjacent stronger IR sources affecting the AllWISE photometry, background galaxies, nebulousity surrounding the source (see Pleiades phenomenon Herbig & Simon 2001, Kalas et al. 2002), and optical/near-infrared binary stars which cannot be resolved with the beam size of WISE. The goal of the image analysis is to eliminate the contamination issues in a quantitative fashion.

The first methodology aims to compare the expected central, cross-correlation position to the position found through isolating the brightest central source in each AllWISE image. When a contamination source is present (at W1 and W2) adjacent to a candidate IR excess star and is unresolved in the AllWISE image, the centroid position of the candidate star shifts. The second methodology is to analyze the isolated source's shape to determine if the object is extended or noncircular. We use a criteria of roundness defined through comparison of the bilateral symmetry of each source determined by fitting a two dimensional gaussian to the source point-spread function defined similar to:

$$Roundness \propto \frac{(\sigma_x - \sigma_y)}{\frac{(\sigma_x + \sigma_y)}{2}} \quad (9)$$

where σ_x and σ_y are the standard deviations of those gaussians. A roundness criteria of zero would appear circular while a roundness of -1.0 or 1.0 would be noticeably elliptical. Further, since we expect W3 and/or W4 excess to be from the dust grains, the disks should be unresolved at the W3 and W4 passbands (except for the nearest stars), hence, their roundness values should be close to zero.

To implement the image inspection, we download $2' \times 2'$ images at each AllWISE passband followed by the source detections on these images using IRAF's program, *daofind*. We compare detected source positions and shapes against the expected stellar positions. All sources were detected in W3, but 770 targets went undetected in W4. Of these non-detections, 92% are cirrus contamination leading to spurious excess fluxes, while the remaining are extended sources indicating large nearby objects, most likely galaxies. The remaining sample contains 3530 sources with identified *daofind* positions in each AllWISE passband that

are plotted in Figure 7 displaying the detected offset between the source position in W3 or W4 compared to W2 since W2 most accurately reflects the Tycho-2 source position. First, we remove sources with positional offsets greater than the resolution of W3 ($6.7''$) or W4 ($12.0''$) in AllWISE. Upon further inspection, however, sources offset in W4 greater than $8.0''$ are also contaminated. Removing 120 sources from offsets in W3 preserves 95% of the sample, but separately, 1180 targets are removed for large offset positions in W4. In this case, 44% of the sources appear to be cirrus, 25% are due to background sources, and the remaining 30% are sources unresolved in the AllWISE images in which the secondary object is brighter at this passband and so shifts the detected source position. Further, excess candidates were inspected for potential ellipticity. Of the 150 sources we remove, 64% appear to be cirrus, 22% are some sort of background object or nebulae, and 14% are likely double stars of similar brightness that are unresolved at W3 or W4. The double stars are removed here because the secondary source will contribute additional flux to the target star and act as a false-positive IR excess candidate. The candidate IR excess stars now total ~ 2100 . Examples of some contaminated targets are displayed in Figure 8.

We mentioned previously, we expect $\sim 6\%$ of the remaining candidates to be giants based on our discussion in Section 3.2.1. With the sample now reduced, we search each candidate position in SIMBAD to identify a published luminosity class or a contaminating object nearby such as a background galaxy. We remove 81 stars with luminosity classes of I, II, or III. Through this endeavor, we also remove 46 other contentious objects such as Cepheid variables, white dwarfs, nebulae, novae, and known galaxies (within $10''$). Additionally, we eliminate 523 sources through inspection of the 2MASS images which display are likely double or multiple star systems (within $10''$) unconfirmed in the AllWISE images, especially W4. Most double stars that are unresolved in the WISE passbands show excess above the photosphere from the over-estimated flux in each passband, and yet still mimics a Rayleigh-Jeans tail. Through inspection of the SED of each star for confirmation or rejection of likely binary-related false excess. The IR excess sample reduces to 1430

stars.

In order to affirm the SED fit and IR excess, we also gather additional photometry through VizieR from the ultraviolet to the far-IR (including data from *Spitzer* MIPS and the *Herschel* PACS or SPIRE instruments; Poglitsch et al. 2010; Griffin et al. 2010) and performed a re-evaluation of the candidate SEDs. Additional photometry did one of three things in terms of contamination or true source identification: 1) it shifts the stellar photosphere slightly such that a star’s significance of excess, now no longer passes our criteria, 2) it provides additional far-IR photospheric data which refutes the AllWISE excess, or 3) it corroborates previous excess detections. Far-IR data from the *Spitzer* MIPS instrument provides better sensitivity through pointed observations, therefore, we treat the *Spitzer* data as representative of the true measurement of far-IR flux. The third case of additional photometry is the only example of beneficial photometry, and so we will examine the other cases in more detail. Firstly, we include more data from the optical and near-IR region of the SEDs from VizieR. More data improves the fit to the stellar photosphere for ~ 80 stars, which shifts the photosphere and the infrared Rayleigh-Jeans tail and a reevaluation of the significance of excess makes these sources non-excess. Secondly, additional photometric measurements at far-IR wavelengths (MIPS, PACS, SPIRE) can reject marginal cases of mid-IR excess. We removed 60 objects with photospheric detections at MIPS 24 and no IR excess at $70\mu\text{m}$. However, one interesting case, HD 69830, found by Beichman et al. (2005b) has mid-IR excess around $10\mu\text{m}$ confirmed using interferometric evidence by Smith et al. (2009b) without the presence of any far-IR excess detection. This rare and unique circumstellar disk is also host to three exoplanets (Lovis et al. 2006). While we do not want to miss any interesting cases, we removed 60 additional stars that have the potential to be HD 69830-like due to true mid-IR excess in W3 and/or W4 and far-IR photospheric detections, since we believe the majority of which are likely bogus excess sources. Our IR excess candidate sample comprises 1230 sources.

3.2.7. Reliability of Excess and Final Distance Restriction

Proximity to our Sun serves as a initial quantifier for our ‘Prime’ targets. We initially selected stars using the total proper motion magnitude as a proxy for a distance corresponding to ~ 200 pc. Considering the size of the Local Bubble and the minor ISM influence on the IR excess in this region, we place stars within 120 pc in our Prime catalog. This identified ~ 300 stars from our Tycho-2/AllWISE IR excess sample with measured distances.

For the remaining 67% of stars without trigonometric parallaxes, we develop a more reliable distance restriction based on a photometric distance calculated by our SED fitting algorithm. The SED fit can use all photospheric photometry for which the brightnesses are highly covariant instead of a single photometric passband. This procedure is based on the final step of the SED fitting algorithm which multiplies the model fluxes by a scale factor, namely $(\frac{R}{d})^2$, where R refers to the stellar radius in solar radii and d is the distance to the star in parsecs (see discussion in Cushing et al. 2008 for more details). We then investigate deducing a distance from this scale factor value using model isochrones to infer an expected stellar radii given the best fit stellar temperature returned from the SED fit. Using the isochrones from Siess et al. (2000), Allard et al. (2011), and Dell’Omodarme et al. (2012), we construct a composite isochrone model which ranges between 2000 and 15000K (for more details regarding this model, see Lee & Song 2016, in prep.). SED distances are estimated for about 900 stars and the expected uncertainties is typically $\sim 12\%$.

The effort to include the SED distance for stars without trigonometric parallax identified 48 stars that are likely evolved M-type stars. Inspection of their SED distance within 15 pc and the total proper motion (less than 40 mas/yr) offers conflicting data regarding the location of these stars. Although there are two small regions (solar apex and anti-apex) where nearby stars exhibit very small proper motions, if the total proper motion is ~ 40 mas/yr, we expect the distance to be on the order of 100 pc. However, for these 48 stars in our sample the SED distances of less than 15 pc are very unrealistic. We retain these stars in the

Reserved sample with an accompanying note until spectroscopy can confirm that they have indeed evolved away from the main sequence.

Finally, to aid in the reliability of our IR excess stellar sample, we generate a parameter called ‘Num.Excess’ in Tables 3 and 4, that represents the number of passbands which display excess above the photosphere. We designate the following wavelength ranges as our IR excess passbands: 5 - 13 μ m, 17 - 30 μ m, 55 - 75 μ m, 90 - 110 μ m, 120 - 170 μ m, 200 - 300 μ m, 300 - 400 μ m, 400 - 500 μ m, 500 - 600 μ m, 700 - 900 μ m, and >1000 μ m. Thus, instruments with similar wavelength photometry such as WISE W4 (22 μ m), *Spitzer* MIPS 24 μ m, and IRAS 25 μ m are maintained as corroborative evidence of the same excess near 25 μ m. Besides being more reliable indication of excess, multiple excess detections reduce the inherent degeneracy in fitting a blackbody to the dust temperature, thereby allowing for a more detailed dust analysis. Tables 3 and 4 will display Num.Excess, the starting wavelength of the IR excess in microns, and a flag if the *Spitzer* IRS spectra is available. These columns should provide a full description of the nature of the excess. We also include in the online materials a table of photometric measurements and model predictions at key stellar fitting passbands for all the stars in Tables 3 and 4 as well as the measured photometry from *Spitzer* and/or *Herschel* if available from the literature. An example of the content and form of the photometry table is provided here in Table 5.

We compare our final tables of Tycho-2/AllWISE Prime IR excess stars and Reserved IR excess candidates with the literature sample found in Section 2 in order to exclude duplicate entries. Then, the following reliability criteria are used as in Section 2 to select reliable IR sources from the Tycho-2/AllWISE sample for our Prime catalog: either

1. at least 2 passbands demonstrating IR excess (‘Num.Excess’>1), AllWISE W3 or W4 flux greater than 10 mJy (for more efficient follow-up observations), and proximity such that distance is within 120 pc;
2. at least 1 passband demonstrating IR excess, AllWISE W3 or W4 flux greater than 10 mJy, has IRS spectra confirming photometric IR excess identification, and distance <120 pc.

Passing the above criteria, we compile just about 500 stars from the Tycho-2/AllWISE search and the literature search for the Prime IR excess catalog. The Reserved table contains over 1200 stars¹.

4. Previous WISE Excess Searches

This study is not the first use of the WISE survey to search for IR excess, therefore we compare our results to the debris disk candidates discovered by Wu et al. (2013), Cruz-Saenz de Miera et al. (2014), Patel et al. (2014), Theissen & West (2014) and Vican & Schneider (2014). We will avoid a comparison between our final samples and Rizzuto et al. (2012) since they made use of the preliminary WISE catalog data only which is now obsolete once the full catalog was released and many of their stars were reassessed through other studies. Each of these searches maintains a similar sample criteria to our new Tycho-2/AllWISE cross-correlation, however, each study presents a different standard of significance of excess and final analysis of the candidates.

First, Wu et al. (2013) was specifically searching for 22 μ m excess using *Hipparcos* stars within 200 pc. They selected candidate excess stars using a color criteria of $[K_S - W4]$ and produced a sample of 141 candidate IR excess stars. Our study was able to reproduce 63 stars from the final Wu et al. (2013) IR excess sample. From the remaining stars that were not matched, 44% have total proper motions according to the Tycho-2 catalog that are less than 25 *mas/yr* (the initial sample selection that we used) and the rest (56%) do not pass our significance of excess.

Patel et al. (2014) found 220 stars showing W3 and/or W4 excess. We confirmed 114 ($\sim 52\%$) of their IR excess stars. Majority (85%) of the remaining 106 IR excess candidates do not pass our significance of excess criteria and the rest (15%) show total proper motions less than 25 *mas/yr* implemented as the initial search criteria of our study.

Constraining their sample using SIMBAD, Cruz-Saenz de Miera et al. (2014) selected only main-sequence dwarfs and any distance. They use

¹The full extent of Tables 3 and 4 are available as online material for this manuscript as well as stored locally on a public server through the University of Georgia entitled: Debris Disk Database (www.debrisdisks.org).

a comparison between the predicted and measured ratio of fluxes (W4/W2) divided by the calibration weighted uncertainty. Through the typical (and somewhat subjective) process of visual inspection of WISE images to remove false-positive IR excess candidates, Cruz-Saenz de Miera et al. (2014) report 197 IR excess stars. We confirmed 40 of these sources as IR excess stars in our Prime or Reserved catalogs. 60% of the Cruz-Saenz de Miera et al. (2014) sample do not pass our significance of excess cut and the remainder (40%) do not pass our total proper motion criteria.

Previous searches for M stars with IR excess by Avenhaus et al. (2012), who used the AllWISE catalog and the RECONS sample from Henry et al. (2006), did not find any new cases of M stars with IR excess indicating a debris disk. Theissen & West (2014) were able to expand this search using the Sloan Digital Sky Survey (SDSS) spectroscopically selected M-type stars out to a distance of nearly 2000 pc. While they executed a series of contamination checks to ensure their sample contains only M dwarfs, only 36% of their 175 IR excess stars are within 200 pc. None of these stars were reproduced by our search. The main reason for the dissimilar results with respect to our sample is distance. Moreover, of the 63 M dwarfs within 200 pc, none of them have Tycho-2 catalog matches. The faintness limit of Tycho-2 would exclude many M dwarfs at these distances.

Vican & Schneider (2014) searched the literature for stars with chromospheric activity indicators in order to constrain the age of their sample before using WISE to determine if these stars had IR excess. Their criteria for excess is very similar to our significance of excess using the comparison between measured and photospheric fluxes, and they found 98 IR excess candidates. Twenty-four of these sources can be found in our Tables 3 and 4. Eight stars were not selected to our sample due to very low total proper motion and the rest (66) were not selected based on our significance of excess criteria.

5. Sample Characteristics

The Prime IR excess star catalog (Table 3) contains ~ 500 stars and information regarding the best fit SED stellar effective temperature, the number of excess passbands, distance, and disk

parameters such as temperature, radius, and fractional dust luminosity. We have marked the previously published IR excess stars using the column “known” that designates one of the star’s first claim of IR excess in the literature. Table 4 mimics the display of the Prime catalog. Most notably, this study has produced >70 new Prime IR excess stars which is almost a 20% increase in notable IR excess stars as well as a handful of very dusty disks ($L_{IR}/L_* \equiv \tau > 10^{-2}$). Further, the number of marginal IR excess stars has quadrupled with this new Tycho-2/AllWISE search.

For the disk parameters, we choose the most simplistic model to define the disk temperature and radius. We assume the SED can first be fit with a single blackbody function. If the single blackbody model does not fit the dust, then a two-blackbody disk model is applied. Stars with *Spitzer* IRS spectroscopy have disk models that match the spectroscopic evidence. In addition, for stars in the Reserved catalog with IR excess in only one passband and without *Spitzer* IRS spectroscopy, we assume a warm dust disk whose dust flux peaks at the single excess wavelength. The fitting parameters are listed in Tables 3 and 4.

Past studies presented several estimates on the occurrence rate of excess stars focusing on nearby, main sequence stars and in some cases focusing on a specific cluster, region, or spectral type. Su et al. (2006) report a debris disk fraction of $\geq 33 \pm 5\%$ surrounding A stars using *Spitzer* MIPS measurements of excess emission at 24 or 70 μm while Beichman et al. (2006b) combined their results with the Bryden et al. (2006a) and Gautier et al. (2007) studies to report $15 \pm 3\%$ of F0 - K0 type stars have debris disks detected at 70 μm . Gorlova et al. (2006) surveyed the 30 Myr old cluster NGC 2547 and report incidences of 40% of B to F type stars demonstrate excess at 24 μm . More recently, Eiroa et al. (2013) discussed the overall prevalence of far-IR detection of circumstellar dust around nearby solar-type stars to be nearly 23%. This can be contrasted with larger all-sky searches for nearby solar-type stars with mid-IR excess such as those performed by Wu et al. (2013) and Patel et al. (2014) who found incidence rates of mid-IR excess specifically at 22 μm solar-type stars of 2.21% and 1.8%, respectively. To create a comparable sample of stars which are not contaminated by nearby objects, we filter the

250,000 starting sample of Tycho-2/AllWISE stars to exclude giants (originally $\sim 30\%$) and then eliminate the expected number of sources with nearby contamination ($\sim 50\%$ of 200,000 stars) extrapolated from the results in Section 3.2.6. This procedure interprets $\sim 120,000$ main sequence stars from various sources that have the potential to contain IR excess stars without any contaminating influences. From this sample, we determine the occurrence of IR excess for Tycho-2/AllWISE stars with W4 excess from the parent sample is 1.0% (1200/120000). In order to best compare with past IR excess studies, we focus on the incidence of $22\ \mu\text{m}$ (W4) excess around A-type or earlier stars and solar-type stars only. Excluding the literature sample from this analysis, we find that 15.6% (~ 320 of 2100 stars with SED temperatures that reflect A-type from the 120000 sample) have infrared excess at W4, while the solar-type stars have an incidence rate for W4 excess of 0.7% ($\sim 850/115000$). This value is in agreement with the values put forth by Wu et al. (2013) and Patel et al. (2014), but still less. We will avoid a discussion of M-type IR excess incidence until spectroscopic evidence indicates a main sequence age.

Considering the spectral types of the Prime and Reserved catalogs, Figure 9 shows the range of the best fit SED stellar temperature. F and G type stars show the largest prevalence of IR excess in these catalogs. Given the sensitivity to detect infrared excess depends on spectral type and distance, the distribution of Prime IR excess stars, especially the apparent concentration of F and G-type stars, is likely an observational bias. However, F and G stars are important for understanding the formation and evolution stellar systems analogous to our Solar System. As a secondary check for our use of the SED effective temperature as a spectral type, we gather spectral type information from SIMBAD where the luminosity class has already been determined (82% of the Prime IR excess catalog). We use the relationship between the spectral type and the SED stellar temperature in order to extrapolate a spectral type for the remaining stars. Without significant outliers, we conclude that our SED fitting algorithm is working effectively. Both Tables 3 and 4 will display the spectral type either with a luminosity class from SIMBAD or with a ‘:’ signifying it is

an interpolated spectral type from SED fits.

We confirm in Figure 10 the representation of IR excess stars across the entire sky. The dashed curve indicates the galactic plane. Stars centered on the galactic plane may show IR excess as the result of source confusion and likely introduce false positives into the sample. However, since the new IR excess stars are not crowded around the galactic plane, we reason that the source confusion did not jeopardize our final catalogs. The two different symbols represent the literature excess sample (triangles) and the new IR excess stars (circles) found here. The small unfilled symbols represent the entire Reserved catalog from Table 4. We note in Figure 10 that there are more candidate IR excess stars at declinations less than -10° and at right ascensions between 150° and 250° . This region highlights the Scorpius-Centaurus Association (ScoCen, hereafter). Based on the age of ~ 11 Myr approximated by Pecaut et al. (2012), we expect this region to have an enhanced density of younger stars with circumstellar material, however, the ages of the ScoCen subregions are still not fully settled (see Herczeg & Hillenbrand 2015). The new IR excess stars that are located near the ScoCen region may be on the forefront of this massive population of young stars.

6. Discussion

We have begun a detailed characterization study of the Prime stars by gathering optical spectroscopy and will be described in a future manuscript studying the relationship between stellar parameters and the dust. Here, we examine the dust parameters in order to investigate relationships between the SED fitting parameters: stellar temperature, dust temperature, dust radius, and the fractional dust luminosity. Lastly, we discuss the relationship between the SED disk radius and the true size of the disk for those disks resolved with scattered light imaging.

6.1. Fractional Dust Luminosity

The fractional dust luminosity defined as $\tau \equiv L_{IR}/L_{star}$, provides an estimate for the amount of dust surrounding each of the IR excess stars regardless of the number of blackbody fits to the dust. Figure 11 shows the distribution of fractional dust luminosity for the Prime catalog (left)

and the Reserved catalog (right). From this distribution, we see that the majority of our main sequence IR excess stars have τ values between 10^{-5} and 10^{-3} . The Reserved sample shows a more central peak around 10^{-3} , although this peak should be evaluated with caution since many of the reserved IR excess stars only display one passband of excess which increases the likelihood of degeneracy in the SED fit to the dust and may select dust temperatures which suggest a higher fractional dust luminosity. Reflecting on our sample, Roberge et al. (2012) explored the sensitivity limits of the fractional dust luminosity of past instruments. However, this investigation of the limiting detectable fractional dust luminosity assumes that each IR excess star has the same amount of dust and is representative of IR excess at far-IR wavelengths. The detectability at mid-IR wavelengths is complicated by the necessity for precise photospheric detections from which to distinguish IR excess and so the limit of mid-IR surveys is more challenging to assess. While not found in our sample and outside of the currently detectable range (i.e. $\tau < 10^{-7}$), we would expect extremely dust poor debris disk systems similar to our solar system ($\tau \sim 10^{-7}$; Wyatt 2008, Moro-Martín et al. 2008, Vitense et al. 2012, Nesvorný et al. 2010). Yet, the other extreme in Figure 11 (i.e. $\tau > 10^{-3}$) provides interesting objects since the amount of dust can either be the result of a large, destructive, transient event such as a period of Late Heavy Bombardment (LHB) or is sustained by the support generated due to presence of gas. A period such as LHB would indicate a mature system that we are able to observe at a crucial planet evolution epoch while the gas may indicate extreme youth.

To compare our new Tycho-2/AllWISE IR excess search with the literature, we plot the fractional dust luminosity against the Johnson visual magnitude in Figure 12. Figure 12 shows our study extends the number of faint stars detected with IR excess. The figure also displays a trend in which these fainter magnitude stars have a higher value of τ . This trend is indicative of later spectral types (K and M) and confirms the observational bias of our survey. The Reserved catalog (right panel of Figure 12) displays the same trend.

Because there are a number of IR excess stars in our catalog with significantly dusty disks ($\tau > 10^{-2}$), we will take a moment just to mention these

Prime catalog targets and some of the associated parameters.

Three stars from the Prime catalog are well-known IR excess sources: HD 98800 (HIP 55505), BD+20 307 (HIP 8920), and HD 141569 (HIP 77542). These stars are within 100 pc and our SED parameters agree with literature values. In particular, HD 98800 was first discovered by Walker & Wolstencroft (1988) and later qualified to be a member of the TW Hydrae association (Zuckerman & Song 2004b), thereby implying the system has an age of roughly 8 Myr but still presents an inner region cleared of gas and dust (Dent et al. 2013). BD+20 307 was first discovered by Song et al. (2005) and then a thorough follow up of mid-IR photometry revealed strong silicate features (Weinberger et al. 2011). The rarity of having a significant amount of warm dust (> 120 K) at > 1 Gyr is indicative of a recent, large collisional event (Song et al. 2005). Finally, HD 141569 is a Herbig Ae star although the nature of the IR excess is still under debate as to whether the disk is more debris disk-like even with the detection of gas in the disk. Either way, the disk was confirmed by Weinberger et al. (1999) using the *Hubble Space Telescope* and so remains one of a few dozen stars which has been resolved through imaging the scattered light.

Besides the very well-known stars, a few other stars have been studied by Chen et al. (2011) and Olofsson et al. (2013). Chen et al. (2006, 2011) reported on the IR excess around HD 146897 (HIP 79977) and HD 129590 (HIP 72070). These solar-type stars are on the edge of our distance restriction but with values of fractional dust luminosity greater than 10^{-2} making them significantly dusty compared to the rest of our Prime catalog stars. In addition, HD 129590 has IRS spectroscopy (Chen et al. 2014) which confirms the amount of dust around this star and the use of a two component disk model fit to the dust. HD 113766 is also best fit with two separate dust temperatures (500 K, 230 K) and Olofsson et al. (2013) performed a full mineralogical investigation into the composition of grains in these disks.

We will address the remaining stars individually since the presentation of the IR excess for these sources are new detections.

TYC 6213-1122-1: This new Tycho-2 IR excess star currently does not have an entry in SIMBAD.

It was best fit with a stellar temperature of 4370 K making it a spectral type of \sim K6. The projected SED distance places this star 60.5 pc from the Earth. In combination with its position at 16 hours right ascension and a declination of -21 degrees, we hypothesize this star may be a new member of the Upper Scorpius-Centaurus region. Figure 13 displays the SED for TYC 6213-1122-1. The youth of this region (\sim 5 Myr; Preibisch & Zinnecker 1999 or \sim 11 Myr; Pecaut et al. 2012) means the large dust emission, $\tau = 23.2 \times 10^{-2}$, may in part be attributed to young age, however, optical spectroscopy is necessary to confirm the age of this system.

TYC 7851-810-1: This star is another new discovery with a similarly dusty disk to TYC 6213-1122-1 and a similar sky position (R.A. of 16 hours, Dec. of -38 degrees) possibly belonging to the Scorpius-Centaurus region. A recent study by Merin et al. (2008) using the *Spitzer* c2d survey which studied “From Molecular Cores to Planet-Forming Disks”, found this object near the ScoCen region and using the MIPS instrument at 24 and $70\mu\text{m}$ qualified the disk to be a young, Class II circumstellar disk. However, based on the shape of the SED, the disk shows a large inner cleared cavity and without information regarding the gas content of the disk, we are led to believe this object is definitely undergoing an interesting transient phase regardless of its age. This object will be discussed further in T. Cotten et al. (2016; in prep). The SED provides a stellar temperature of 4590K (\sim K6 spectral type), $\tau = 13.1 \times 10^{-2}$, and a distance of 57.6 pc. From Figure 13, the IR excess is corroborated by photometry at AllWISE W3 and W4, IRAS 25, 60, and $100\mu\text{m}$, *Spitzer* MIPS 24, 70, and $160\mu\text{m}$.

TYC8830-410-1: This star does not have any available information or references from SIMBAD. It is best fit using a 4900 K stellar temperature and so we assign it a spectral type of K3. The dust displays a luminosity of $\tau = 1.90 \times 10^{-2}$ in the warm inner region near the star and is best fit using a single disk with a dust temperature of 425 K. Our SED returned a distance of 120 pc for this source. Based on the evidence we have for this star, the IR excess is indicative of the rare case of warm debris such as with BD+20 307. Based on the knowledge that silicates are expected to emit around $10\mu\text{m}$, the peak of this star’s IR excess at W3 (see Figure

13) could indicate a transient event which is generating the destruction of planetesimals, comets, and/or asteroids. Current ongoing observations using SOFIA (Stratospheric Observatory for Infrared Astronomy; Young et al. 2012; cycle 3 & 4 programs 03_0099, 04_0126, 04_0130) should provide more evidence regarding the nature of the dust.

6.2. Dust Temperatures and Disk Radii

The parameters of the dust fits can be used to derive an orbital dust radius (R_{disk}) as in Rhee et al. (2007). This implies that $R_{\text{disk}}(R_{\odot}) = (\frac{R_{*,\text{SED}}}{2})(\frac{T_{*,\text{SED}}}{T_{\text{disk}}})^2$ which is then converted into AU. If the true dust grains are smaller than the model blackbody grains, they would be located further away than blackbody grains. Figure 14 displays the dust temperature and radius of disk. The symbol shapes distinguish between a single or two-component disk fit by using a connecting solid line. Over one third of the Prime IR excess stars have disks (\sim 37%) are best fit using two blackbody curves. The left plot displays the Prime catalog stars while the right shows the Reserved catalog restricted to stars that have more than one IR excess passband. These top plots show no recognizable trend for spectral type and dust temperature which directly agrees with the reports mentioned in the review article by Matthews et al. (2014). Thus, we conclude that the luminosity and mass of the host star does not predict the temperature expected for the micron-sized grains creating the IR excess. However, the dust temperature is not the complete picture and is intimately linked to the disk radius.

Considering the results shown in the top panels of Figure 14, the bottom panels confirm a trend of late-type stars having the smallest disk radii. If all spectral types sustain disks of similar dust temperatures, then the late-type stars would need to have dust closer to the star to reradiate IR excess at the same temperature as early-type stars. In addition, the estimated silicate grain sublimation range (\sim 1500 K estimated by Moro-Martin 2013) is plotted as the red dashed line in Figure 14. Because dust grains will be sublimated inside of this range, we do not see any IR excess stars with disk size smaller than this in our catalogs. We note, however, that for a given stellar spectral type, the smallest disk size is at least an order of

magnitude larger than the dust sublimation limit. This implies that either grains far from the sublimation distance are efficiently removed by other mechanisms or that hot disks are not identifiable observationally because of the various limits (e.g., photospheric flux estimate, poor photometric measurement of excess emission, etc.).

The dust temperature for the stars fit with a single dust temperature using multiple passbands of IR excess from the Prime and Reserved catalogs is shown in Figure 15. The distribution of dust temperatures appears to be evenly spread with a peak around 200 K. This peak mostly reflects the IR excess stars whose excess begins around W3 and peaks in the mid-IR. Since many of these disks are new discoveries using AllWISE and may not have far-IR photometry, our distribution may be biased in that many disks may only show the warm tail end of the dust disk. Separately, previous discoveries of IR excess make up the majority of the population of disks with cooler dust temperatures around 80 K. This is due to the fact that the known IR excess stars were mainly discovered at far-IR wavelengths where the excess begins at or after W4.

Figure 16 compares the fractional dust luminosity to the dust radius. The temperatures of the single blackbody fits and the two components of the dust are plotted as the color in the figure. One may expect that an IR excess star with multiple disk components would exhibit a higher fractional dust luminosity, but Figure 16 does not display such a trend. Additionally, this figure confirms that the warm disk components are closer to the star, while the cooler components are further away. This plot does display an apparent void of low fractional dust luminosity and small disk radius. As referenced earlier, this deficit of stars is likely an observational bias due to the difficulty in assessing IR excess from the photosphere at wavelengths shorter than $10\mu\text{m}$ which may produce a collection of marginal, warm IR excess stars.

Studies of thermally resolved disks by Booth et al. (2013) and Rodriguez & Zuckerman (2012) found that the predicted disk radius from the SED blackbody fit was 1-5 times smaller than the size of the disk resolved in thermal imaging. They conclude from their results that the dust grains studied using different techniques must be of different sizes and compositions and in particular,

thermal imaging better traces the larger grains. Scattered light imaging probes a small grain size (sub-micron) and yet this ratio has been used to compare this method to the SED disk radius. In Figure 17, we display the predicted disk radius from our blackbody SED fit to the disk radius for stars that have been resolved through scattered light. There are over two dozen of these stars in our catalogs and they have been identified in the tables. A few of the most well-known debris disk stars have been labeled in the figure including AU Mic, Fomalhaut, and beta Pictoris. Figure 17 shows that we can make a prediction regarding the relationship between different dust detection methods. The SED disk radii (shown as black squares) displays the trend shown by the best-fit solid black line and the additional lines shown in this figure are multiplicative factors of this line. Since many of the disks are extended, we include the inner and outer components of the continuous disk rather than an average or peak location of the dust. This plot demonstrates the resolved inner disk boundary ranges from 1 to 4 times the blackbody disk radius in agreement with the results from Rodriguez & Zuckerman (2012) and Booth et al. (2013). Further, we extend this relationship to the outer edge of the dust disks and estimate the outer edge of the circumstellar material can extend to nearly 20 times the blackbody dust radius.

Biases between the disks resolved through scattered light and SED blackbody modeling complicate the comparison made in Figure 17. For many disks imaged in scattered light, the inner portion of the disk suffers from self-subtraction due to the large stellar flux and so an inner rim is difficult to measure. On the far side, the dust grains tend to fade out of view of the central star's flux at large distances and so an outer rim is difficult to determine as well. Further, the inclination angle of the disk presents difficulties in determining an inner and outer edge, especially if the disk is edge-on like AU Mic. In these cases, the inner rim of the dust is approximated by the closest the scattered light technique can probe to the central star. The comparison shown in Figure 17 is still useful as it can be extrapolated to the entire Prime catalog and used as a method to identify targets for future observations and improve predictions regarding the expected dust location.

7. Conclusion

We have conducted an extensive search and collection of IR excess stars from two sources: a new Tycho-2 cross-correlation with the AllWISE catalog and a literature search for previously claimed IR excess stars. We recognize a need for a saturation correction in AllWISE W2 and develop a simple polynomial correction. Using a SED fitting algorithm, we determine the amount of excess above the photosphere comparing the measured and the photospheric fluxes. We select new IR excess candidates by requiring an excess of $> 3\sigma$ or $> 5\sigma$ in either W3 or W4 and infrared bright in either W3 or W4 (> 10 mJy). Further, extensive analysis of the AllWISE images removed a large number of false-positives. We then implement a series of criteria involving brightness, number of passbands showing excess, and distance in order to ensure a sample of the highest fidelity IR excess stars displaying an SED indicative of a post-protoplanetary disk. For stars lacking an accurate *Hipparcos* parallax, we perform an estimate of distance using the best fit SED temperature and extrapolating a typical stellar radius from a composite isochrone. This is similar to a photometric distance, but with improved accuracy using all the available photometric data from the optical to infrared wavelengths. Finally, the inclusion of catalogs such as *Akari*, IRAS, AllWISE, *Spitzer* MIPS, IRAS, and *Herschel* PACS and SPIRE improves the reliability of the Prime catalog, especially when the measurements corroborate and reduce the degeneracy of the SED fitting algorithm.

Specifically focusing on our Prime sample of ~ 500 nearby (< 120 pc) IR excess stars, we have compiled the largest, most reliable IR excess star catalog to date. In addition, the new Tycho-2/AllWISE search for IR excess increased the known, reliable IR excess sample by $\sim 20\%$. Moreover, a few IR excess stars appear to be new, extremely dusty systems requiring follow-up observations to better understand the evolution of the dust and/or the transient nature of the dust. The literature IR excess sample represents mainly the cold, less dusty disks, while the newly discovered Tycho-2/AllWISE IR excess stars are typically warmer and more dusty. Considering the Reserved sample, this study more than doubled the number of known IR excess stars and these stars

are maintained for more sensitive future surveys.

We offer a discussion of the relationship between the dust parameters and stellar parameters obtained during the SED fitting procedure and a portrayal of many two disk systems which span the entire spectral type range. Our findings affirm that a two component dust disk does not suggest any particular stellar or dust temperature, but also that the activity which generates the dust around these stars can be assumed to be analogous to either the Asteroid or the Kuiper belt and operates regardless of the luminosity or mass of the host star. Future work should strive for a complete catalog of sub millimeter data which has been shown to be more suggestive of the true amount of dust in these systems and thus, provide a better suggestion of the mass of dust in each system. In addition, we investigate the relationship between the disk radius assumed using a blackbody disk model and the disk radius resolved using scattered light. Since scattered light reveals the actual location of dust in the disk, the SED disk radius can be used to indicate that the true inner disk radius is roughly four times larger and the outer disk radius is twenty times larger than predicted by the SED.

We thank the referee for their very helpful comments and suggestions that have improved this manuscript. Support for this work was provided by NASA (NNN12AA01C, NAS2-97001) through an award issued by JPL/Caltech and USRA as well as partially supported by a grant issued by SOFIA and USRA to UGA. The authors would also like to acknowledge J. Lee, A. Schneider, and L. Sgro for their helpful suggestions. This study has made extensive use of the NASA/IPAC Infrared Science Archive, data products from the Wide-field Infrared Survey Explorer, the *Herschel* Science archive, the *Spitzer* Heritage Archive, SIMBAD, and VizieR (operated at CDS).

REFERENCES

- Absil, O., di Folco, E., Merand, A. et al., 2008, A&A, 487, 1041.
- Acke, B., Min, M., Dominik, C., 2012, A&A, 540, 125.
- Akeson, R. L., Ciardi, D. R., Millan-Gabet, R. et al., 2009, ApJ, 691, 1896.
- Ardila, D. R., Van Dyk, S. D., Makowiecki, W. et al., 2010, ApJS, 191, 301.

- Aumann, H. H., Beichman, C. A., Gillett, F. C. et al., 1984, *ApJ*, 278L, 23.
- Allard, F., Homeier, D. & Freytag, B., 2011, *ASPC*, 448, 91.
- Avenhaus, H., Schmid, H. M., & Meyer, M. R., 2012, *A&A*, 548, 105.
- Bailey, V., Meshkat, T., Reiter, M. et al., 2014, *ApJ*, 780, 4.
- Ballering, N. P., Rieke, G. H., Su, K. Y. L., & Montiel, E., 2013, *ApJ*, 775, 55.
- Ballering, N. P., Rieke, G. H., & Gaspar, A., 2014, *ApJ*, 793, 57.
- Balog, Z., Kiss, L. L., Vinko, J. et al., 2009, *ApJ*, 698, 1989.
- Barber, S. D., Patterson, A. J., Kilic, M. et al., 2012, *ApJ*, 760, 26.
- Beichman, C. A., Neugebauer, G., Habing, H. J. et al., 1988, *IRAS catalogs and atlases. Volume 1: Explanatory supplement*.
- Beichman, C. A., Bryden, G., Rieke, G. H. et al., 2005, *ApJ*, 622, 1160.
- Beichman, C. A., Bryden, G., Gautier, T. N. et al., 2005, *ApJ*, 626, 1061.
- Beichman, C. A., Tanner, A., Bryden, G. et al., 2006a, *ApJ*, 639, 1166.
- Beichman, C. A., Bryden, G., Stapelfeldt, K. R. et al., 2006b, *ApJ*, 652, 1674.
- Beuzit, J.-L., Feldt, M., Dohlen, K. et al., 2008, *SPIE*, 7014, 701418.
- Bessell, M. S. & Brett, J. M., 1988, *PASP*, 100, 1134.
- Bessell, M. S., 2000, *PASP*, 112, 961.
- Bitner, M. A., Chen, C. H., Muzerolle, J. et al., 2010, *ApJ*, 714, 1542.
- Bonsor, A. & Wyatt, M., 2010, *MNRAS*, 409, 1631.
- Bonsor, A., Kennedy, G. M., Crepp, J. R. et al., 2013, *MNRAS*, 431, 3025.
- Bonsor, A., Kennedy, G. M., Crepp, J. R. et al., 2014, *MNRAS*, 437, 3288.
- Booth, M., Wyatt, M. C., Morbidelli, A. et al., 2009, *MNRAS*, 399, 385.
- Booth, M., Kennedy, G., Sibthorpe, B. et al., 2013, *MNRAS*, 428, 1263.
- Broekhoven-Fiene, H., Matthews, B. C., Kennedy, G. M. et al., 2013, *ApJ*, 762, 52.
- Brown, J. M., Blake, G. A., Qi, C. et al., 2008, *ApJ*, 675, 109.
- Brown, J. M., Blake, G. A., Qi, C. et al., 2009, *ApJ*, 704, 496.
- Bryden, G., Beichman, C. A., Trilling, D. E. et al., 2006a, *ApJ*, 636, 1098.
- Bryden, G., Beichman, C. A., Rieke, G. H. et al., 2006b, *ApJ*, 646, 1038.
- Bryden, G., Beichman, C. A., Carpenter, J. M. et al., 2009, *ApJ*, 705, 1226.
- Buenzli, E., Thalmann, C., Vigan, A. et al., 2010, *A&A*, 524, 1.
- Bulger, J., Hufford, T., Schneider, A. et al., 2013, *ApJ*, 636, 1098.
- Carpenter, J. M., Mamajek, E. E., Hillenbrand, L. A. et al., 2006, *ApJ*, 651, 49.
- Carpenter, J. M., Mamajek, E. E., Hillenbrand, L. A. & Meyer, M. R., 2009, *ApJ*, 705, 1646.
- Carpenter, J. M., Ricci, L. & Isella, A., 2014, *ApJ*, 787, 42.
- Chen, C. H., Jura, M., Gordon, K. D. et al., 2005a, *ApJ*, 623, 493.
- Chen, C. H., Patten, B. M., Werner, M. W. et al., 2005b, *ApJ*, 634, 1372.
- Chen, C. H., Sargent, B. A., Bohac, C. et al., 2006, *ApJS*, 166, 351.
- Chen, C. H., Fitzgerald, M. P. & Smith, P. S., 2008, *ApJ*, 689, 539.
- Chen, C. H., Mamajek, E. E., Bitner, M. A. et al., 2011, *ApJ*, 738, 122.
- Chen, C. H., Pecaut, M., Mamajek, E. E. et al., 2012, *ApJ*, 756, 133.
- Chen, C. H., Mittal, T., Kuchner, M. et al., 2014, *ApJS*, 211, 25.
- Churcher, L. J., Wyatt, M. C. & Smith, R., 2011a, *MNRAS*, 410, 2.
- Churcher, L. J., Wyatt, M. C., Duchene, G. et al., 2011b, *MNRAS*, 417, 1715.
- Cieza, L. A., Kessler-Silacci, J. E., Jaffe, D. T. et al., 2005, *ApJ*, 635, 422.
- Cieza, L., Padgett, D. L., Stapelfeldt, K. R. et al., 2007, *ApJ*, 667, 308.
- Cieza, L., Cochran, W. D., & Augereau, J.-C., 2008, *ApJ*, 679, 720.
- Cieza, L. A., Schreiber, M. R., Romero, G. A. et al., 2010, *ApJ*, 712, 925.
- Cieza, L. A., Schreiber, M. R., Romero, G. A. et al., 2012, *ApJ*, 750, 157.
- Cloutier, R., Currie, T., Rieke, G. H. et al., 2014, *ApJ*, 796, 127.
- Cruz-Saenz de Miera, F., Chavez, M., Bertone, E. et al., 2014, *MNRAS*, 437, 391.
- Cutri, R. M., Wright, E. L., Conrow, T. et al., 2012, *Explanatory Supplement to the WISE All-Sky Data Release Products*, Tech rep.
- Cutri, R. M., Wright, E. L., Conrow, T. et al., 2013, *Explanatory Supplement to the AllWISE Data Release Products*, Tech rep.
- Currie, T., Lisse, C. M., Sicilia-Aguilar, A. et al., 2011, *ApJ*, 734, 115.
- Cushing, M. C., Marley, M. S., Saumon, D. et al., 2008, *ApJ*, 678, 1372.
- Dahm, S. E., Slesnick, C. L., & White, R. J., 2012, *ApJ*, 745, 56.

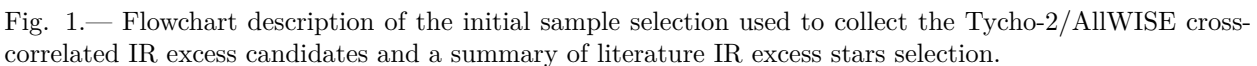
- Decin, G., Dominik, C., Malfait, K. et al., 2000, *A&A*, 357, 533.
- Dell’Omodarme, M., Valle, G., Degl’Innocenti, S. et al., 2012, *A&A*, 540, 26.
- Dent, W. R. F., Thi, W. F., Kamp, I. et al., 2013, *PASP*, 125, 477.
- Desidera, S., Covino, E., Messina, S. et al., 2011, *A&A*, 529, 54.
- Donaldson, J. K., Roberge, A., Chen, C. H. et al., 2012, *ApJ*, 753, 147.
- Duchene, G., McCabe, C., Pinte, C. et al., 2010, *ApJ*, 712, 112.
- Eiroa, C., Fedele, D., Maldonado, J. et al., 2010, *A&A*, 518, 131.
- Eiroa, C., Marshall, J. P., Mora, A. et al., 2011, *A&A*, 536, 4.
- Eiroa, C., Marshall, J. P., Mora, A. et al., 2013, *A&A*, 555, 11.
- Ertel, S., Wolf, S., Marschall, J. P. et al., 2012, *A&A*, 541, 148.
- Esplin, T. L., Luhman, K. L., & Mamajek, E. E., 2014, *ApJ*, 784, 126.
- Fujiwara, H., Yamashita, T., Ishihara, D. et al., 2009a, *ApJ*, 695, 88.
- Fujiwara, H., Ishihara, D., Kataza, H. et al., 2009b, *ASP Conference Series*, 418, 109.
- Fujiwara, H., Ishihara, D., Onaka, T. et al., 2013, *A&A*, 550, 45.
- Gardner, J. P., Mather, J. C., Clampin, M. et al., 2006, *Space Sci. Rev.*, 123, 485.
- Gaspar, A., Rieke, G. H., Su, K. Y. L. et al., 2009, *ApJ*, 697, 1578.
- Gaspar, A., Rieke, G. H., & Balog, Z., 2013, *ApJ*, 768, 25.
- Gautier, T. N. III, Rieke, G. H., Stansberry, J. et al., 2007, *ApJ*, 667, 527.
- Gautier, T. N. III, Rebull, L. M., Stapelfeldt, K. R. et al., 2008, *ApJ*, 683, 813.
- Gizis, J. E., 2010, *arXiv:1008.4576*.
- Golimowski, D. A., Krist, J. E., Stapelfeldt, K. R. et al., 2011, *AJ*, 142, 30.
- Gorlova, N., Padgett, D. L., Rieke, G. H. et al., 2004, *ApJS*, 154, 448.
- Gorlova, N., Rieke, G. H., Muzerolle, J. et al., 2006, *ApJ*, 649, 1028.
- Gorlova, N., Balog, Z., Rieke, G. H. et al., 2007, *ApJ*, 670, 516.
- Goto, M., Usuda, T., Dullemond, C. P. et al., 2006, *ApJ*, 652, 758.
- Greaves, J. S., Wyatt, M. C., Holland, W. S., & Dent, W. R. F., 2004, *MNRAS*, 351, 54.
- Greaves, J. S., Holland, W. S., Wyatt, M. C. et al., 2005, *ApJ*, 619, 187.
- Greaves, J. S., Wyatt, M. C. & Bryden, G., 2009, *MNRAS*, 397, 757.
- Greaves, J. S. & Wyatt, M. C., 2010, *MNRAS*, 404, 1944.
- Greaves, J. S., Kennedy, G. M., Thureau, N. et al., 2014a, *MNRAS*, 438, 31.
- Greaves, J. S., Sibthorpe, B., Acke, B. et al., 2014b, *ApJ*, 791, 11.
- Gregorio-Hetem, J., Lepine, J. R. D., Quast, G. R. et al., 1992, *AJ*, 103, 549.
- Griffin, M. J., Abergel, A., Abreu, A. et al., 2010, *A&A*, 518, 3.
- Grinin, V. P., Potravnov, I. S. & Musaev, F. A., 2010, *A&A*, 524, 8.
- Guieu, S., Pinte, C., Monin, J.-L. et al., 2007, *A&A*, 465, 855.
- Gutermuth, R. A., Megeath, S. T., Myers, P. C. et al., 2009, *ApJS*, 184, 18.
- Hauschildt, P. H., Allard, F., & Baron, E., 1999, *ApJ*, 512, 377.
- Heng, K., 2011, *MNRAS*, 415, 3365.
- Henry, T. J., Jao, W.-C., Subasavage, J. P. et al., 2006, *AJ*, 132, 2360.
- Hernandez, J., Briceno, C., Calvet, N. et al., 2006, *ApJ*, 652, 472.
- Hernandez, J., Hartmann, L., Megeath, T. et al., 2007, *ApJ*, 662, 1067.
- Hernandez, J., Hartmann, L., Calvet, N. et al., 2008, *ApJ*, 686, 1195.
- Hernandez, J., Calvet, N., Hartmann, L. et al., 2009, *ApJ*, 707, 705.
- Herbig, G. H. & Simon, T., 2001, *AJ*, 121, 3138.
- Herczeg, G. J. & Hillenbrand, L. A., 2015, *ApJ*, 808, 23.
- Hillenbrand, L. A., Carpenter, J. M., Kim, J. S. et al., 2008, *ApJ*, 677, 630.
- Hines, D. C., Backman, D. E., Bouwman, J. et al., 2006, *ApJ*, 638, 1070.
- Høg, E., Fabricius, C., Makarov, V. V. et al., 2000, *A&A*, 355, 19.
- Hung, L.-W., Duchene, G., Arriaga, P. et al., 2015, *ApJ*, 815, 14.
- Jang-Condell, H., Chen, C. H., Mittal, T. et al., 2015, *ApJ*, 808, 167.
- Janson, M., Brandt, T. D., Moro-Martin, A. et al., 2013, *ApJ*, 773, 73.
- Jayawardhana, R., Coffeey, J., Scholz, A. et al., 2006, *ApJ*, 648, 1206.
- Jarrett, T. H., Cohen, M., Masci, F. et al., 2011, *ApJ*, 735, 112.
- Jourdain de Muizon, M., Laureijs, R. J., Dominik, C. et al., 1999, *A&A*, 350, 875.
- Jura, M., 1991, *ApJ*, 383, 79.
- Jura, M., Chen, C. H., Furlan, E. et al., 2004, *ApJS*, 154, 453.

- Kalas, P., Graham, J. R., Beckwith, S. V. W. et al., 2002, *ApJ*, 567, 999.
- Kalas, P., Graham, J. R., Clampin, M. C. et al., 2006, *ApJ*, 637, 57.
- Kalas, P., Fitzgerald, M. P., & Graham, J. R., 2007a, *ApJ*, 661, 85.
- Kalas, P., Duchene, G., Fitzgerald, M. P. et al., 2007b, *ApJ*, 671, 161.
- Kastner, J. H., Zuckerman, B., Hily-Blant, P. et al., 2008, *A&A*, 492, 469.
- Kastner, J. H., Hily-Blant, P., Sacco, G. G. et al., 2010, *ApJ*, 723, 248.
- Kennedy, G. M. & Wyatt, M. C., 2010, *MNRAS*, 405, 1253.
- Kennedy, G. M. & Wyatt, M. C., 2011, *MNRAS*, 417, 2281.
- Kennedy, G. M., Wyatt, M. C., Sibthorpe, B. et al., 2012, *MNRAS*, 426, 2115.
- Kennedy, G. M., Wyatt, M. C., Kalas, P. et al., 2014a, *MNRAS*, 438, 96.
- Kennedy, G. M., Murphy, S. J., Lisse, C. M. et al., 2014b, *MNRAS*, 438, 3299.
- Kenyon, S. J. & Bromley, B. C., 2008, *ApJS*, 179, 451.
- Kim, J. S., Hines, D. C., Backman, D. E. et al., 2005, *ApJ*, 632, 659.
- Koerner, D. W., Kim, S., Trilling, D. E. et al., 2010, *ApJ*, 710, 26.
- Kospal, A., Ardila, D. R., Moor, A. et al., 2009, *ApJ*, 700, 73.
- Krautter, J., Wichmann, R., Schmitt, J. H. M. M. et al., 1997, *A&AS*, 123, 329.
- Krivov, A. V., 2010, *Research in Astronomy and Astrophysics*, 10, 383.
- Lafreniere, D., Doyon, R., Marois, C. et al., 2007, *ApJ*, 670, 1367.
- Laureijs, R. J., Jourdain de Muizon, M., Leech, K. et al., 2002, *A&A*, 387, 285.
- Lagrange, A.-M., Bronnefoy, M., Chauvin, G. et al., 2010, *Science*, 329, 57.
- Lawler, S. M., Beichman, C. A., Bryden, G. et al., 2009, *ApJ*, 705, 89.
- Lawler, S. M. & Gladman, B., 2012, *ApJ*, 752, 53.
- Lebreton, J., Augereau, J.-C., Thi, W.-F. et al., 2012, *A&A*, 539, 17.
- Lestrade, J.-F., Wyatt, M. C., Bertoldi, F. et al., 2006, *A&A*, 460, 733.
- Lestrade, J.-F., Wyatt, M. C., Bertoldi, F. et al., 2009, *A&A*, 506, 1455.
- Lestrade, J.-F., Matthews, B. C., Sibthorpe, B. et al., 2012, *A&A*, 548, 86.
- Liseau, R., Eiroa, C., Fedele, D. et al., 2010, *A&A*, 518, 132.
- Lisse, C. M., Beichman, C. A., Bryden, G. et al., 2007, *ApJ*, 658, 584.
- Liu, M. C., Matthews, B. C., Williams, J. P. et al., 2004, *ApJ*, 608, 526.
- Liu, Q., Wang, T. & Jiang, P., 2014, *AJ*, 148, 3.
- Lovis, C., Mayor, M., Pepe, F. et al., 2006, *Nature*, 331, 305.
- Low, F. J., Smith, P. S., Werner, M. et al., 2005, *ApJ*, 631, 1170.
- Luhman, K. L., Adame, L., D’Allesio, P. et al., 2007, *ApJ*, 666, 1219.
- Luhman, K. L. & Mamajek, E. E., 2012, *ApJ*, 758, 31.
- Lyo, A.-R., Lawson, W. A., Mamajek, E. E. et al., 2003, *MNRAS*, 338, 616.
- Macintosh, B., Graham, J., Palmer, D. et al., 2006, *SPIE*, 6272, 62720L.
- Maldonado, J., Eiroa, C., Villaver, E. et al., 2012, *A&A*, 541, 40.
- Maldonado, J., Eiroa, C., Villaver, E. et al., 2015, *A&A*, 579, 20.
- Mamajek, E. E., Meyer, M. R., Hinz, P. M. et al., 2004, *ApJ*, 612, 496.
- Maness, H. L., Kalas, P., Peek, K. M. G. et al., 2009, *ApJ*, 707, 1098.
- Mannings, V. & Barlow, M. J., 1998, *ApJ*, 497, 330.
- Marois, C., Macintosh, B., Barman, T. et al., 2008, *Science*, 322, 1348.
- Marshall, J. P., Lohne, T., Montesinos, B. et al., 2011, *A&A*, 529, 117.
- Marshall, J. P., Moro-Martin, A., Eiroa, C. et al., 2014, *A&A*, 565, 15.
- Mathews, G. S., Pinte, C., Duchene, G. et al., 2013, *A&A*, 558, 66.
- Matthews, B. C., Kalas, P. G. & Wyatt, M. C., 2007a, *ApJ*, 663, 1103.
- Matthews, B. C., Greaves, J. S., Holland, W. S. et al., 2007b, *PASP*, 119, 842.
- Matthews, B. C., Sibthorpe, B., Kennedy, G. et al., 2010, *A&A*, 518, 135.
- Matthews, B. C., Krivov, A. V., Wyatt, M. C., Bryden, G., & Eiroa, C., 2014, in *Protostars and Planets VI*, eds. H. Beuther, R. Klessen, C. Dullemond & T. Henning.
- Melis, C., Zuckerman, B., Song, I., et al., 2009, *ApJ*, 696, 1964.
- Melis, C., Zuckerman, B., Rhee, J. H. et al., 2010, *ApJ*, 717, L57.
- Melis, C., Zuckerman, B., Rhee, J. H. et al., 2012, *Nature*, 487, 74.
- Melis, C., Zuckerman, B., Rhee, J. H. et al., 2013, *ApJ*, 778, 12.
- Meng, H. Y. A., Rieke, G. H., Su, K. Y. L. et al., 2012, *ApJ*, 751, 17.
- Merin, B., Jorgensen, J., Spezzi, L. et al., 2008, *ApJS*, 177, 551.

- Metchev, S. A., Hillenbrand, L. A. & Meyer, M. R., 2004, *ApJ*, 600, 435.
- Metchev, S. A., Marois, C. & Zuckerman, B., 2009, *ApJ*, 705, 204.
- Meyer, M. R., Carpenter, J. M., Mamajek, E. E. et al., 2008, *ApJ*, 673, 181.
- Millan-Gabet, R., Serabyn, E., Mennesson, G. et al., 2011, *ApJ*, 734, 67.
- Mizusawa, T. F., Rebull, L. M., Stauffer, J. R. et al., 2012, *AJ*, 144, 135.
- Moerchen, M. M., Telesco, C. M., Packham, C. et al., 2007a, *ApJ*, 655, 109.
- Moerchen, M. M., Telesco, C. M., De Buizer, J. M. et al., 2007b, *ApJ*, 666, 109.
- Moerchen, M. M., Telesco, C. M. & Packham, C., 2010, *ApJ*, 723, 1418.
- Monin, J.-L., Guieu, S., Pinte, C. et al., 2010, *A&A*, 515, 91.
- Moor, A., Abraham, P., Derekas, A. et al., 2006, *ApJ*, 644, 525.
- Moor, A., Apai, D., Pascucci, I. et al., 2009, *ApJ*, 700, 25.
- Moor, A., Pascucci, I., Kospal, A. et al., 2011, *ApJS*, 193, 4.
- Moor, A., Juhasz, A., Kospal, A., 2013, *ApJ*, 777, 25.
- Moor, A., Kospal, A., Abraham, P. et al., 2015, *MNRAS*, 447, 577.
- Morales, F. Y., Werner, M. W., Bryden, G. et al., 2009, *ApJ*, 699, 1067.
- Morales, Farisa Y., Rieke, G. H., Werner, M. W., 2011, *ApJ*, 730, L29.
- Morales, Farisa Y., Padgett, D., Bryden, G. et al., 2012, *ApJ*, 757, 7.
- Morales, F. Y., Bryden, G., Werner, M. W. et al., 2013, *ApJ*, 776, 111.
- Moro-Martin, A., Carpenter, J. M., Meyer, M. R. et al., 2007, *ApJ*, 658, 1312.
- Moro-Martin, A., Malhotra, R., Carpenter, J. M. et al., 2007a, *ApJ*, 668, 1165.
- Moro-Martin, A., Wyatt, M. C., Malhotra, R., Trilling, D. E., 2008, In *The Solar System Beyond Neptune*, ed. A. Barucci et al., 465.
- Moro-Martin, A., Malhotra, R., Bryden, G. et al., 2010, *ApJ*, 717, 1123.
- Moro-Martin, A., 2013, In *Planets, Stars and Stellar Systems*, ed. Oswalt, T. et al., 431.
- Najita, J. & Williams, J. P., 2005, *ApJ*, 635, 625.
- Nesvorný, D., Jenniskens, P., Levison, H. F. et al., 2010, *ApJ*, 713, 816.
- Nilsson, R., Liseau, R., Brandeker, A. et al., 2009, *A&A*, 508, 1057.
- Nilsson, R., Liseau, R., Brandeker, A. et al., 2010, *A&A*, 518, 40.
- Olofsson, J., Henning, Th., Nielbock, M. et al., 2013, *A&A*, 551, 134.
- Oudmaijer, R. D., van der Veen, W. E. C. J., Waters, L. B. F. M. et al., 1992, *A&AS*, 96, 625.
- Panic, O., Holland, W. S., Wyatt, M. C. et al., 2013, *MNRAS*, 435, 1037.
- Panic, O., Ratzka, Th., Mulders, G. D. et al., 2014, *A&A*, 562, 101.
- Patel, Rahul I., Metchev, S. A., & Heinze, A., 2014, *ApJS*, 212, 10.
- Patience, J., Bulger, J., King, R. et al., 2011, *A&A*, 531, 17.
- Patten, B. M. & Willson, L. A., 1991, *AJ*, 102, 323.
- Pawellek, N., Krivov, A. V., Marshall, J. P. et al., 2014, *ApJ*, 792, 65.
- Pecaut, M. J., Mamajek, E. E. & Bubar, E. J., 2012, *ApJ*, 746, 154.
- Peterson, D. E., Caratti o Garatti, A., Bourke, T. L. et al., 2011, *ApJS*, 194, 43.
- Pilbratt, G. L., Riedinger, J. R., Passvogel, T. et al., 2010, *A&A*, 518, L1.
- Plavchan, P., Werner, M. W., Chen, C. H. et al., 2009, *ApJ*, 698, 1068.
- Poglitsch, A., Waelkens, C., Geis, N. et al., 2010, *A&A*, 518, 2.
- Preibisch, T. & Zinnecker, H., 1999, *AJ*, 117, 2381.
- Rebull, L. M., Stapelfeldt, K. R., Werner, M. W. et al., 2008, *ApJ*, 681, 1484.
- Rebull, L. M., Padgett, D. L., McCabe, C.-E. et al., 2010, *ApJS*, 186, 259.
- Riaz, B., Mullan, D. J. & Gizis, J. E., 2006, *ApJ*, 650, 1133.
- Riaz, B. & Gizis, J. E., 2012, *A&A*, 548, 54.
- Ricci, L., Testi, L., Natta, A. et al., 2014, *ApJ*, 791, 20.
- Reid, I. N., Turner, E. L., Turnbull, M. C. et al., 2007, *ApJ*, 665, 767.
- Rieke, G. H., Su, K. Y., Stansberry, J. A. et al., 2005, *ApJ*, 620, 1010.
- Riviere-Marichalar, P., Menard, F., Thi, W. F. et al., 2012a, *A&A*, 538, 3.
- Riviere-Marichalar, P., Barrado, D., Augereau, J.-C. et al., 2012b, *A&A*, 546, 8.
- Riviere-Marichalar, P., Pinte, C., Barrado, D. et al., 2013, *A&A*, 555, 67.
- Riviere-Marichalar, P., Barrado, D., Montesinos, B. et al., 2014, *A&A*, 565, 68.
- Rizzuto, A. C., Ireland, M. J., & Zucker, D. B., 2012, *MNRAS*, 421, 97.
- Rhee, J. H., Song, I., Zuckerman, B., & McElwain, M., 2007, *ApJ*, 660, 1556.
- Rhee, J. H., Song, I., & Zuckerman, B., 2007b, *ApJ*, 671, 616.
- Rhee, J. H., Song, I., & Zuckerman, B., 2008, *ApJ*, 675, 777.

- Roberge, A. & Weinberger, A. J., 2008, *ApJ*, 676, 509.
- Roberge, A., Chen, C. H., Millan-Gabet, R. et al., 2012, *PASP*, 124, 799.
- Roccatagliata, V., Henning, Th., Wolf, S. et al., 2009, *A&A*, 497, 409.
- Rodigas, T. J., Hinz, P. M., Leisenring, J. et al., 2012, *ApJ*, 752, 57.
- Rodigas, T. J., Debes, J. H., Hinz, P. M. et al., 2014, *ApJ*, 783, 21.
- Rodigas, T. J., Stark, C. C., Weinberger, A. et al., 2015, *ApJ*, 798, 96.
- Rodriguez, D. R. & Zuckerman, B., 2012, *ApJ*, 745, 147.
- Sadakane, K. & Nishida, M., 1986, *PASP*, 98, 685.
- Saffe, C. & Gomez, M., 2004, *A&A*, 423, 221.
- Schneider, A., Song, I., Melis, C. et al., 2012, *ApJ*, 757, 163.
- Schneider, A., Song, I., Melis, C. et al., 2013, *ApJ*, 777, 78.
- Schneider, G., Weinberger, A. J., Becklin, E. E. et al., 2009, *AJ*, 137, 53.
- Sicilia-Aguilar, A., Bouwman, J., Juhasz, A. et al., 2009, *ApJ*, 701, 1188.
- Siegler, N., Close, L. M., Burgasser, A. J. et al., 2007, *AJ*, 133, 2320.
- Sierchio, J. M., Rieke, G. H., Su, K. Y. L. et al., 2010, *ApJ*, 712, 1421.
- Siess L., Dufour E., Forestini M., 2000, *A&A*, 358, 593.
- Silverstone, M. D., Meyer, M. R., Mamajek, E. E. et al., 2006, *ApJ*, 639, 1138.
- Smith, P. L., Hines, D. C., Low, F. J. et al., 2006, *ApJ*, 644, 125.
- Smith, R., Wyatt, M. C. & Dent, W. R. F., 2008, *A&A*, 485, 897.
- Smith, R., Churcher, L. J., Wyatt, M. C. et al., 2009, *A&A*, 493, 299.
- Smith, R., Wyatt, M. C. & Haniff, C. A., 2009b, *A&A*, 503, 265.
- Smith, R. & Wyatt, M. C., 2010, *A&A*, 515, 95.
- Smith, R., Jeffries, R. D., & Oliveira, J. M., 2011, *MNRAS*, 411, 2186.
- Smith, R. & Jeffries, R. D., 2012, *MNRAS*, 420, 2884.
- Spangler, S. R., Sargent, A. I., Silverstone, M. D. et al., 2001, *ApJ*, 555, 932.
- Song, I., Caillault, J.-P., Barrado y Navascues, D. et al., 2001, *ApJ*, 546, 352.
- Song, I., Weinberger, A. J., Becklin, E. E. et al., 2002, *AJ*, 124, 514.
- Song, I., Zuckerman, B., Weinberger, A. J. et al., 2005, *Nature*, 436, 363.
- Soummer, R., Perrin, M. D., Pueyo, L. et al., 2014, *ApJ*, 786, 23.
- Stock, N. D., Su, K. Y. L., Liu, W. et al., 2010, *ApJ*, 724, 1238.
- Su, K. Y. L., Rieke, G. H., Misselt, K. A. et al., 2005, *ApJ*, 628, 487.
- Su, K. Y. L., Rieke, G. H., Stansberry, J. A. et al., 2006, *ApJ*, 653, 675.
- Su, K. Y. L., Rieke, G. H., Stapelfeldt, K. R. et al., 2008, *ApJ*, 679, 125.
- Su, K. Y. L., Rieke, G. H., Stapelfeldt, K. R. et al., 2009, *ApJ*, 705, 314.
- Sylvester, R. J., Dunkin, S. K., & Barlow, M. J., 2001, *MNRAS*, 327, 133.
- Tanner, A., Beichman, C., Bryden, G. et al., 2009, *ApJ*, 704, 109.
- Thalmann, C., Janson, M., Buenzli, E. et al., 2013, *ApJ*, 763, 29.
- Theissen, C. & West, A., 2014, *ApJ*, 794, 146.
- Thompson, M. A., Smith, D. J. B., Stevens, J. A. et al., 2010, *A&A*, 518, 134.
- Thureau, N. D., Greaves, J. S., Matthews, B. C. et al., 2014, *MNRAS*, 445, 2558.
- Trilling, D. E., Stansberry, J. A., Stapelfeldt, K. R. et al., 2007, *ApJ*, 658, 1289.
- Trilling, D. E., Bryden, G., Beichman, C. A. et al., 2008, *ApJ*, 674, 1086.
- Urban, L. E., Rieke, G., Su, K. et al., 2012, *ApJ*, 750, 98.
- van Leeuwen, F., 2007, *A&A*, 474, 653.
- Vandenbussche, B., Sibthorpe, B., Acke, B. et al., 2010, *A&A*, 518, 133.
- Vican, L. & Schneider, A., 2014, *ApJ*, 780, 154.
- Vitense, C., Krivov, A. V., Kobayashi, H. et al., 2012, *A&A*, 540, 30.
- Wahhaj, Z., Cieza, L., Koerner, D. W. et al., 2010, *ApJ*, 724, 835.
- Wahhaj, Z., Liu, M. C., Nielsen, E. L. et al., 2013, *ApJ*, 773, 179.
- Walker, H. J. & Wolstencroft, R. D., 1988, *PASP*, 100, 1509.
- Weinberger, A. J., Becklin, E. E., Schneider, G. et al., 1999, *ApJ*, 525, 66.
- Weinberger, A. J., Beklin, E. E. & Zuckerman, B., 2003, *ApJ*, 584, 33.
- Weinberger, A. J., 2008, *ApJ*, 679, 41.
- Weinberger, A. J., Becklin, E. E., Song, I. et al., 2011, *ApJ*, 726, 72.
- Williams, J. P. & Andrews, S. M., 2006, *ApJ*, 653, 1480.
- Williams, J. P. & Cieza, L. A., 2011, *ARA&A*, 49, 67.
- Wilner, D. J., Andrews, S. M. & Hughes, A. M. et al., 2011, *ApJ*, 727, 42.
- Wittenmyer, R. A., Tan, X., Lee, M. H. et al., 2014, *ApJ*, 780, 140.
- Wright, E. L., Eisenhardt, P., Mainzer, A. et al., 2010, *AJ*, 140, 1868.
- Wu, Chao-Jian, Wu, Hong, Lam, Man-I. et al., 2013, *ApJS*, 208, 29.

- Wyatt, M. C., Dent, W. R. F. & Greaves, J. S., 2003, MNRAS, 342, 876.
- Wyatt, M. C., Smith, R., Greaves, J. S. et al., 2007a, ApJ, 658, 569.
- Wyatt, M. C., Smith, R., Su, K. Y. L. et al., 2007, ApJ, 663, 365.
- Wyatt, Mark C., 2008, ARA&A, 46, 339.
- Wyatt, M. C., Kennedy, G., Sibthorpe, B. et al., 2012, MNRAS, 424, 1206.
- Wyatt, M. C., PaniÄŒ, O, Kennedy, G. M. et al., 2015, *Ap&SS*, 357, 103.
- Young, E. T., Beckline, E. E., Marcum, P. M. et al., 2012, ApJ, 749, 17.
- Zuckerman, B., 2001, ARA&A, 39, 549.
- Zuckerman, B. & Song, I., 2004b, ARA&A, 42, 685.
- Zuckerman, B. & Song, I., 2004a, ApJ, 603, 738.
- Zuckerman, B., Rhee, J. H., Song, I. et al., 2011, ApJ, 732, 61.
- Zuckerman, B., Melis, C., Rhee, J. H. et al., 2012, ApJ, 752, 58.
- Zuckerman, B., & Song, I., 2012, ApJ, 758, 77.



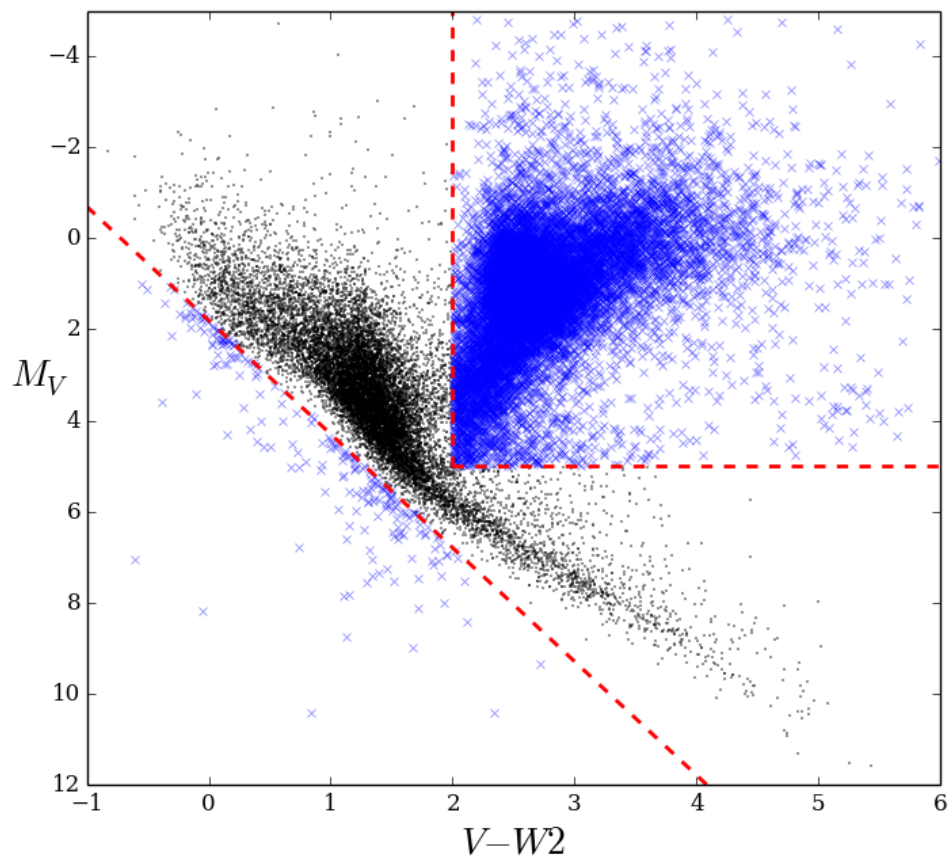


Fig. 2.— Color-magnitude diagram for the Tycho-2/AllWISE stars with *Hipparcos* parallax information. The dashed lines designate the cuts for removing giants and white dwarfs. We have selected this line to ensure we do not lose many main sequence dwarfs. The blue ‘x’ symbols constitute over 15000 stars rejected from the cross-correlated sample for being giants or white dwarfs.

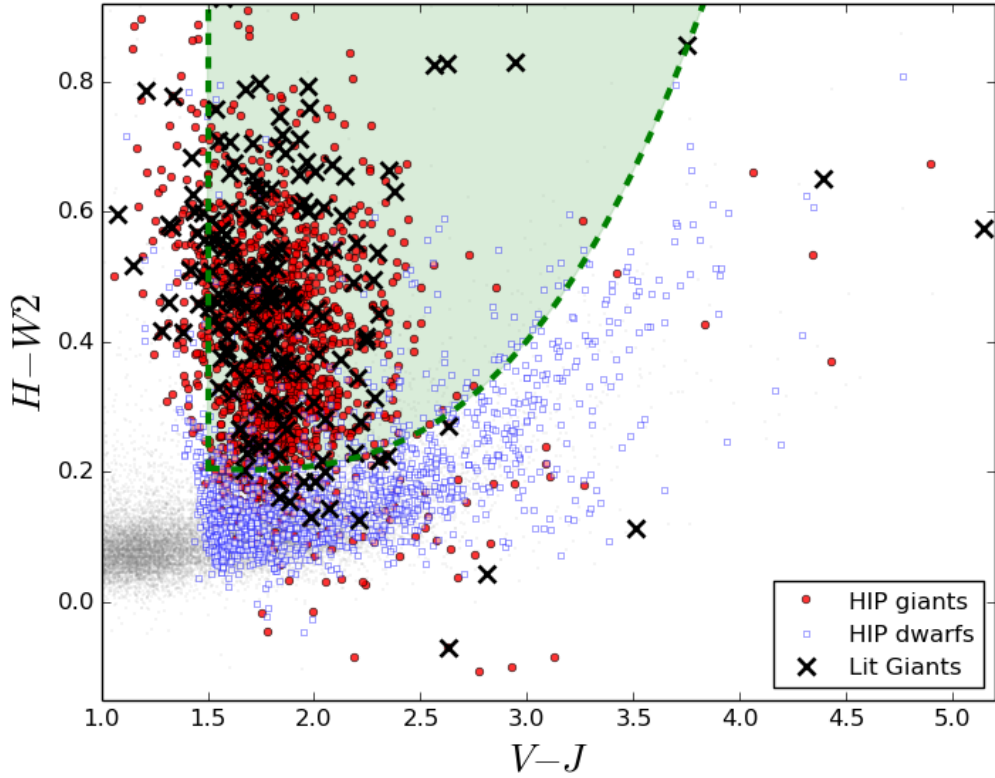


Fig. 3.— Color-color diagram used to distinguish giant stars. The green dashed curves and the enclosed shaded region displays the cuts used in removing additional late-type evolved stars from our main sequence sample (see Section 3.2.1 for the functional form of the curved line). The small grey dots are the remaining sample of $> 200,000$ Tycho-2 stars. The red circles are the *Hipparcos* giants removed from the sample using the CMD (see Figure 2), while the blue, unfilled squares are the *Hipparcos* main sequence sample selected in the CMD that have well-measured parallax (error $< 10\%$). The large ‘X’ symbols are giants selected from SIMBAD which have a luminosity class of I, II, or III.

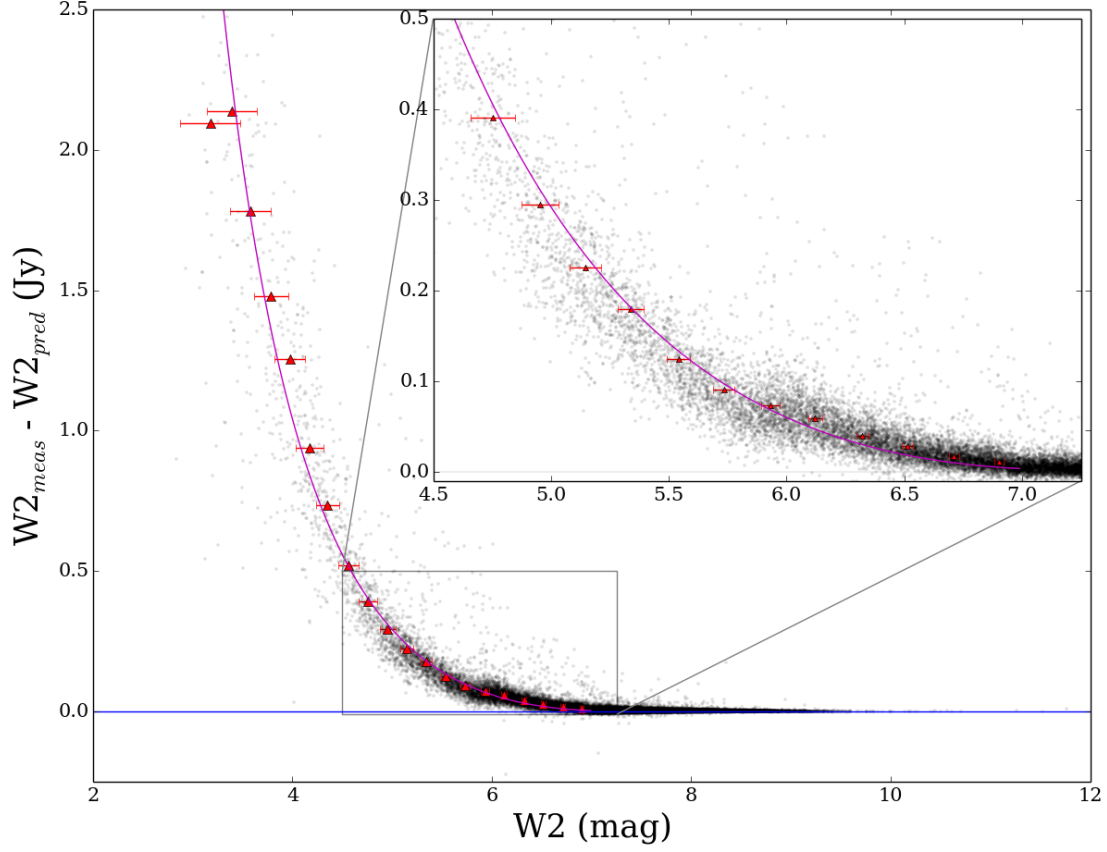


Fig. 4.— The function displayed is designed to correct the flux over-estimation effect in AllWISE W2 passband. The data plotted contains stars with effective temperatures from the SED fitting greater than 6000K, binned by ~ 0.2 magnitudes, and fit using a series of logarithms in the saturation region. A solid (blue) horizontal line has been displayed at zero for reference. The correction function is of the form: $y(Jy) = 3.28 - 168.55 \times \log(x + 0.084)^{-1} + 164.78 \times \log(x + 0.003)^{-1}$ and applies to W2 magnitudes less than 7.

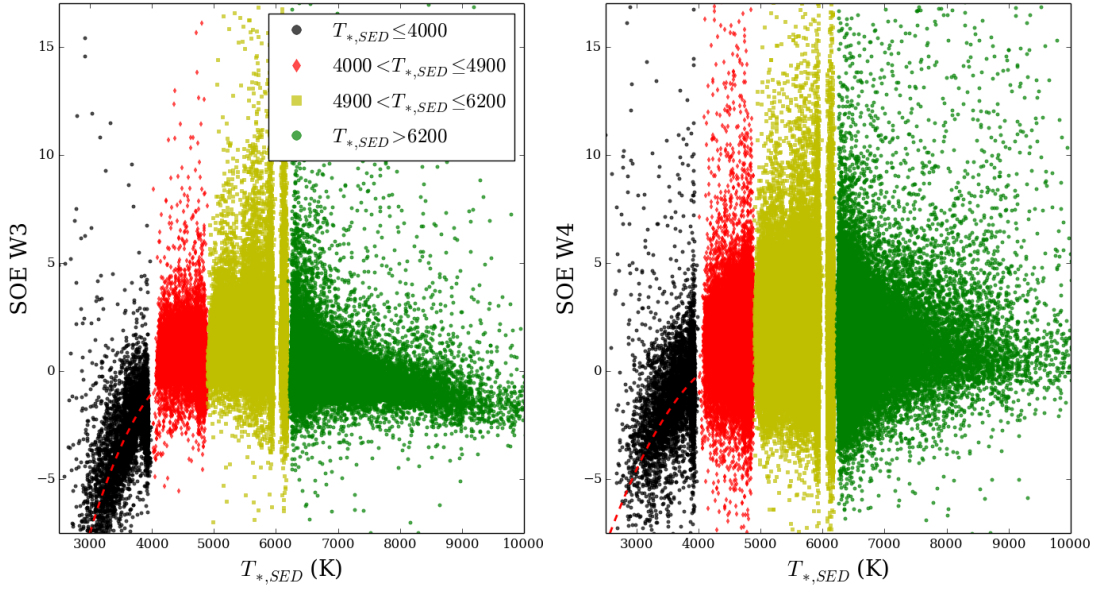


Fig. 5.— *Left*: Significance of excess in AllWISE W3 flux for stars in the cross-correlated sample (243,354) versus the best fit stellar temperature from the SED. The colors represent four different regions pointing out the trend towards ‘negative excess’ of the coolest stars in our sample. This trend is seen for stars with SED temperatures less than 4000K and is fitted with a function shown as the dashed line (Refer to Section 3.2.5: Equations 7 and 8 for the functional form of the corrections). *Right*: Same as the left plot for AllWISE W4.

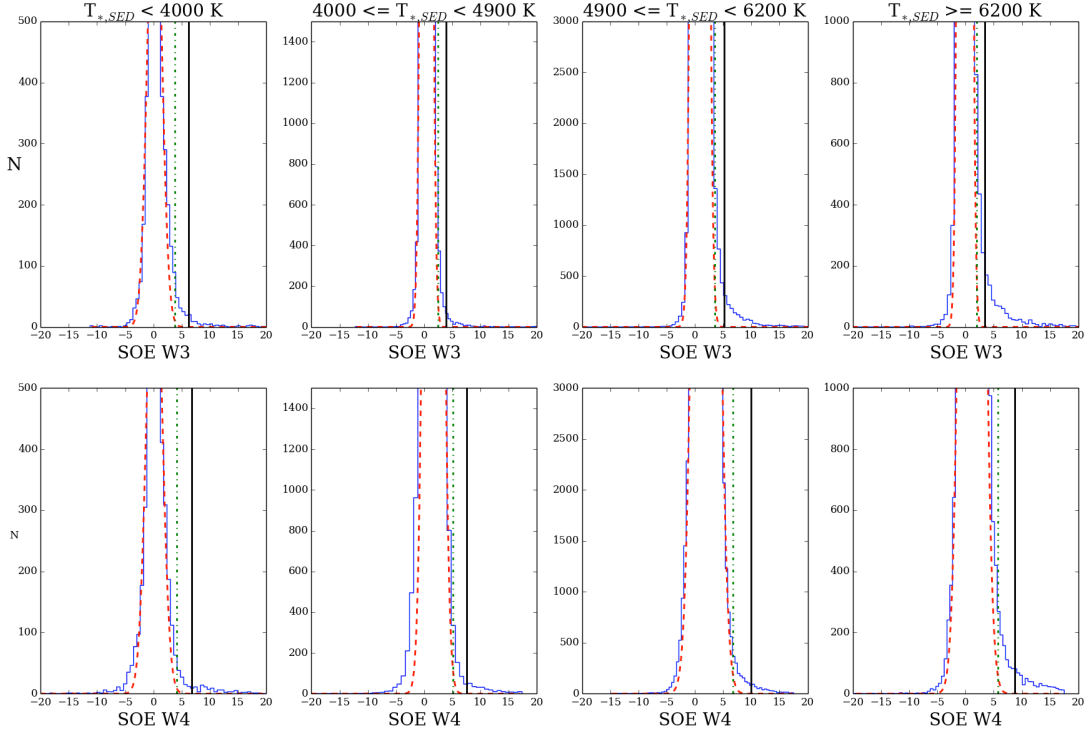


Fig. 6.— Significance of excess for the temperature divisions shown in Figure 5. Each histogram portrays our significance of excess defined in Section 3.2.5 and is fitted with a Gaussian and the green (dot-dashed) and black (solid) vertical lines represent the 3σ and 5σ selection criteria for excess stars, respectively. The histograms have been magnified to show the true distribution of stars within each temperature division.

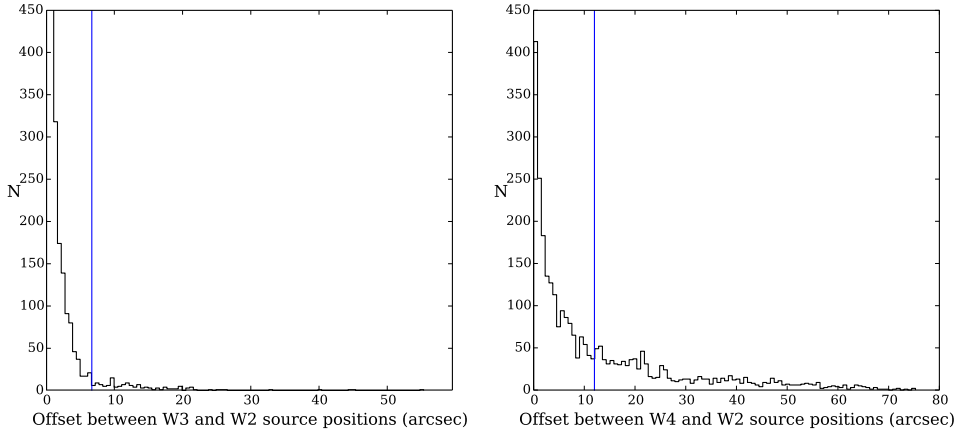


Fig. 7.— Offset in the main source position between AllWISE W2 and W3 (*Left*) and W2 and W4 (*Right*). The difference between W2 and W3 do not show a significant variation from which to distinguish contamination. The difference between W2 and W4 shows a larger spread and can easily distinguish cases of image contamination. We have initially removed stars further separated than $6.7''$ in W3 or $12.0''$ in W4 using the resolution of WISE as a cutoff. The vertical lines indicate this location. (See text for more details.)

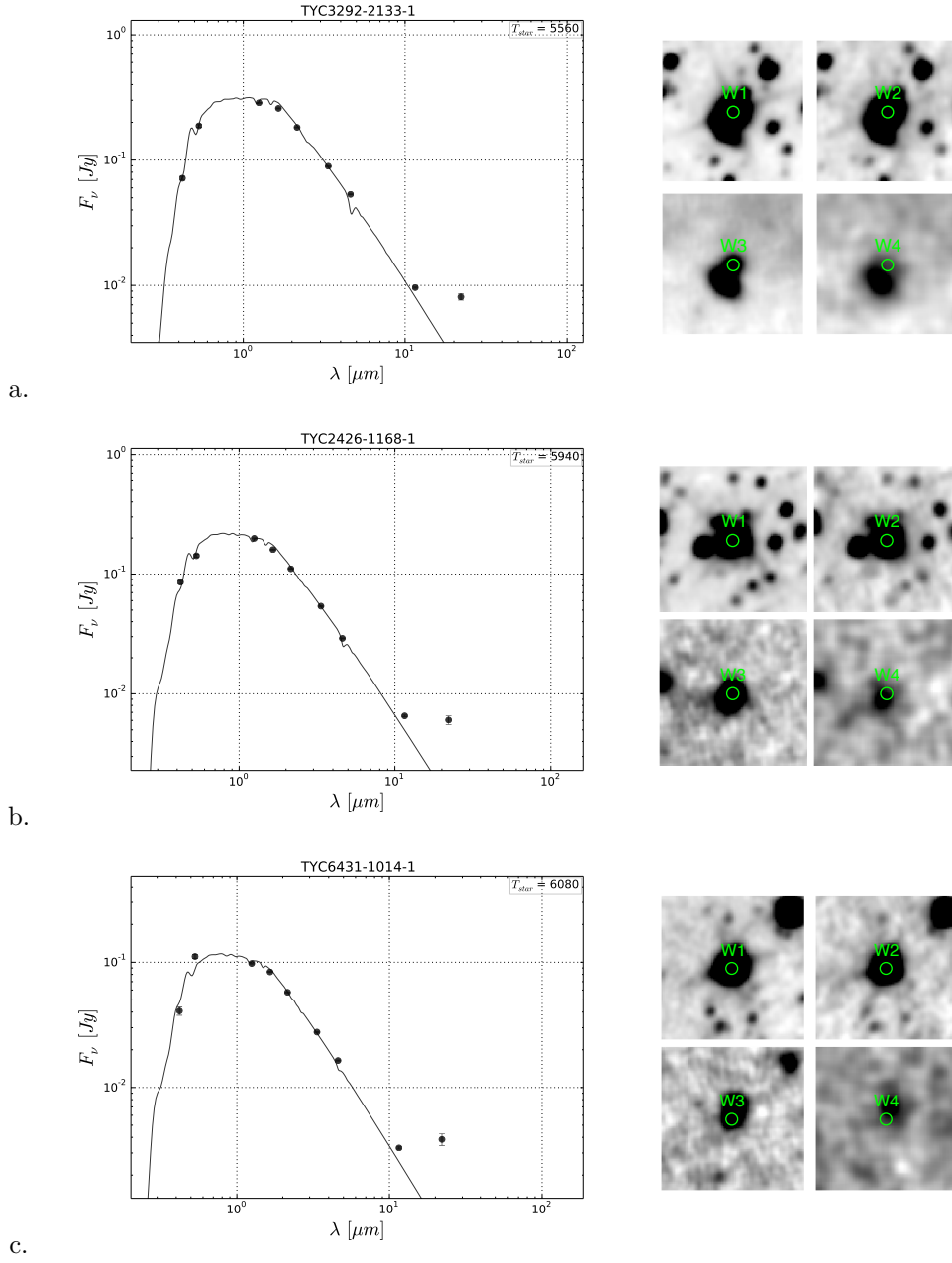


Fig. 8.— This figure shows examples of stars removed during the image vetting procedures. The *left-hand* figure displays the SED for each star with the photosphere fit to Tycho-2 B_T , V_T , 2MASS J, H and K_S . The *right-hand* figure shows the AllWISE images taken from the NASA/IPAC Infrared Science Archive and are $2'$ by $2'$, scaled linearly. The images also contain a $5.0''$ circle centered on the search position. a.) Due to both the background contaminating cirrus and the large offset to the brightest source in W4, this source is likely a background galaxy found through our offset criteria. b.) This source passed the initial offset criteria, but further inspection proved sources with W4 offsets $> 8.0''$ needs to be removed as well. The object shown in the W4 image is offset from the W2 position by $9.1''$ and yet the amount of W4 excess emission cannot be due to a center source alone. c.) This source demonstrates an elliptical shape in W3, this source is rejected based on the roundness criteria and is likely a background IR source. See Section 3.2.6 for more details regarding these images.

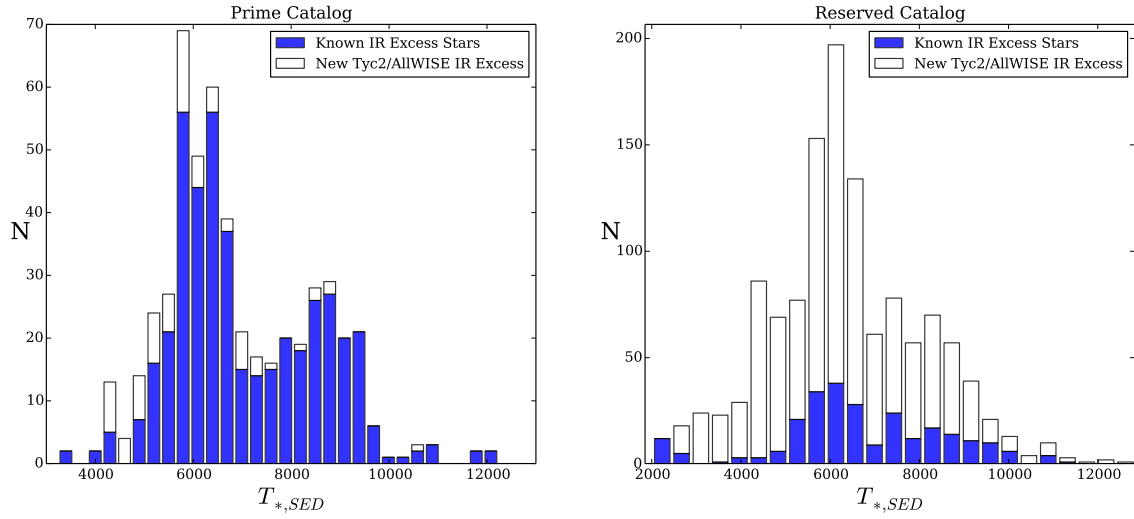


Fig. 9.— Distribution of best fit stellar temperature in the final, Prime IR excess sample (*Left*) and the Reserved sample (*Right*). The filled histogram contains stars previously claimed to display IR excess and reproduced in this study. The unshaded histogram contains stars which are new IR excess detections from our Tycho-2/AllWISE search. Refer to Section 5 for more details.

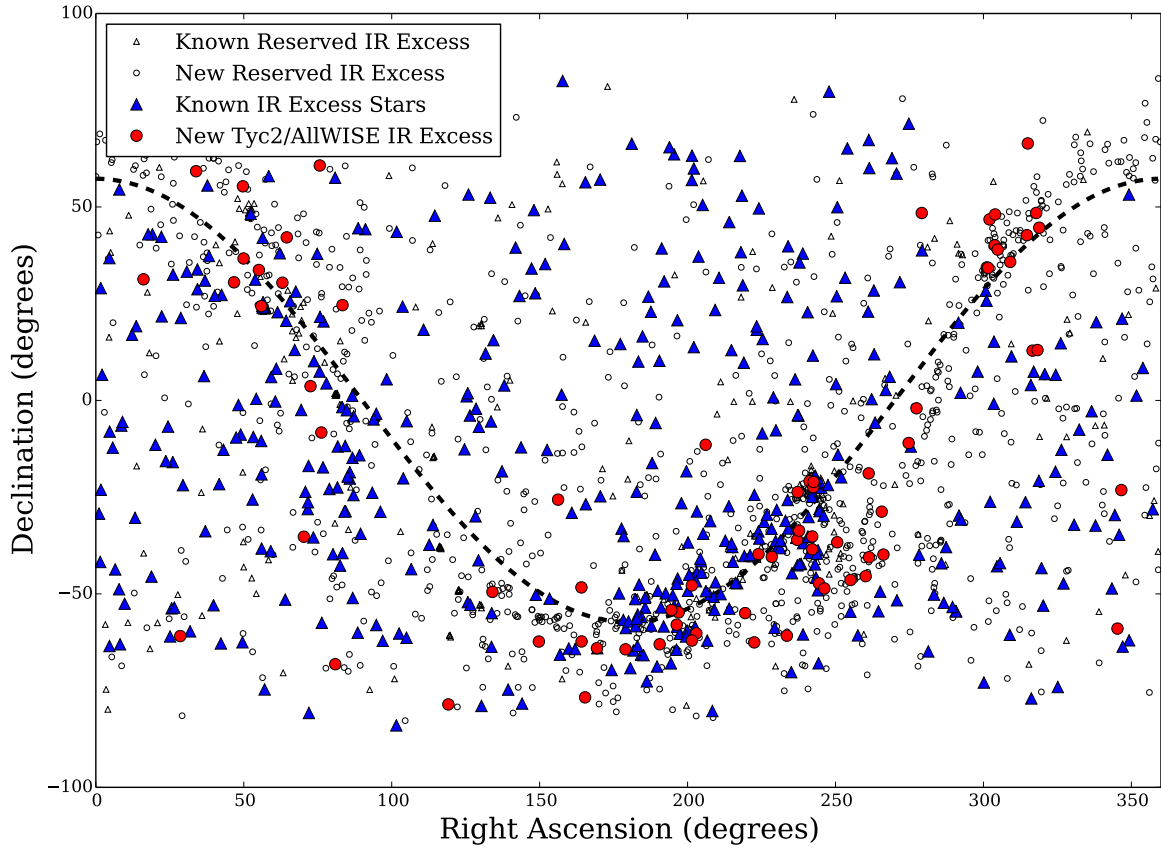


Fig. 10.— Spatial distribution of IR excess stars in R.A. and Dec. Red circles represent the new, Prime Tycho-2/AllWISE IR excess stars and blue triangles show the sample of known, Prime IR excess stars. The grey symbols are from the Reserved catalog that did not qualify for the Prime targets. The symbol shapes are the same for the literature and new IR excess stars in the Reserved sample. For reference, the dashed curve signifies the galactic plane.

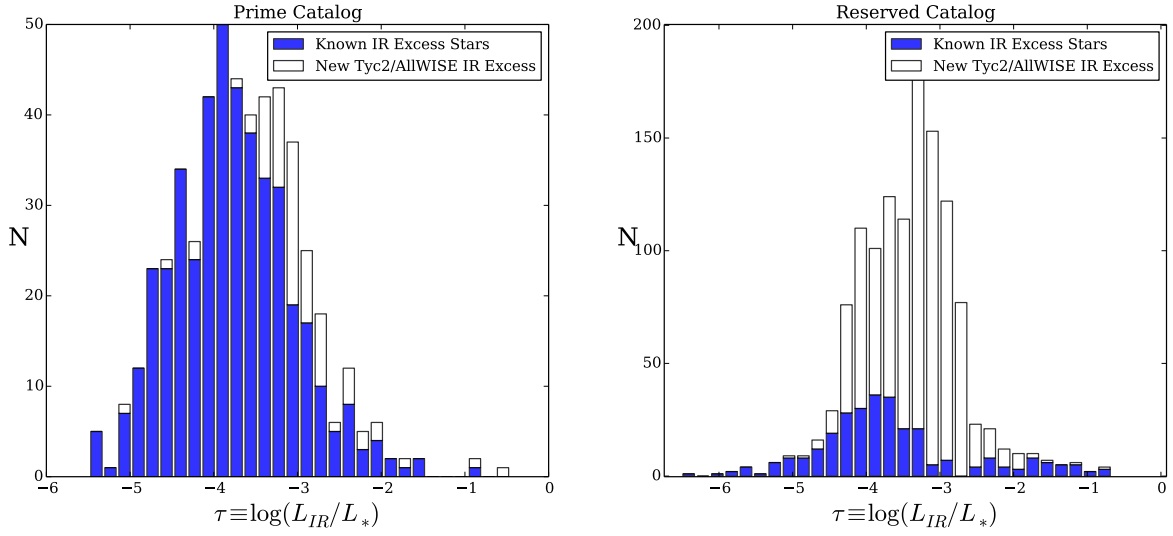


Fig. 11.— Histogram of the fractional dust luminosity displayed in logarithmic scale for the Prime IR excess catalog (*left*) and the Reserved catalog (*right*). The average fractional dust luminosity for the Prime catalog has a value of $10^{-3.8}$ where low τ stars were not detected due to limited sensitivities of IR excess surveys. There are a handful of extremely dusty disks ($\tau > 10^{-2}$) which will be interesting for further understanding the formation and evolution of dust around a star.

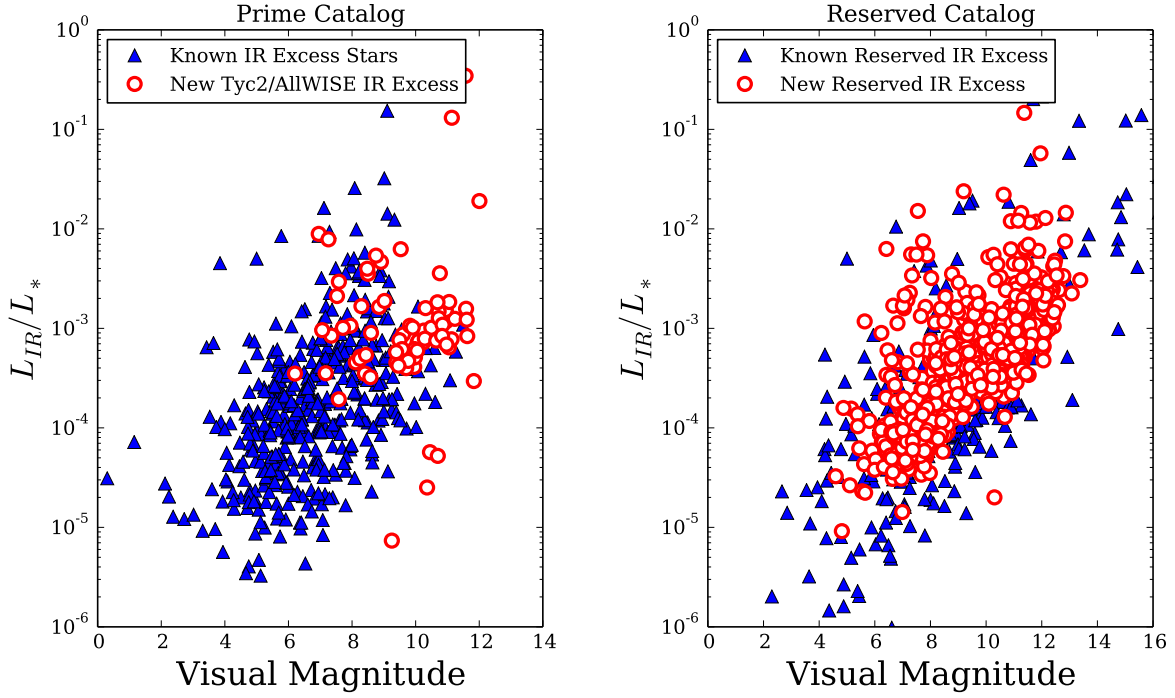


Fig. 12.— Visual magnitude versus the fractional dust luminosity for the Prime IR excess stars (left) and the Reserved Catalog (right). This plot demonstrates that our new Prime IR excess stars extend to fainter magnitudes as the sensitivity of instruments has improved. The Reserved catalog covers the same range of magnitudes. There are a handful of very dusty disks ($\tau > 10^{-1}$) in the Reserved catalog, however, the majority of these stars are likely the population of remaining giants in the sample based on an SED distance within 15 pc (see Section 3.2.7).

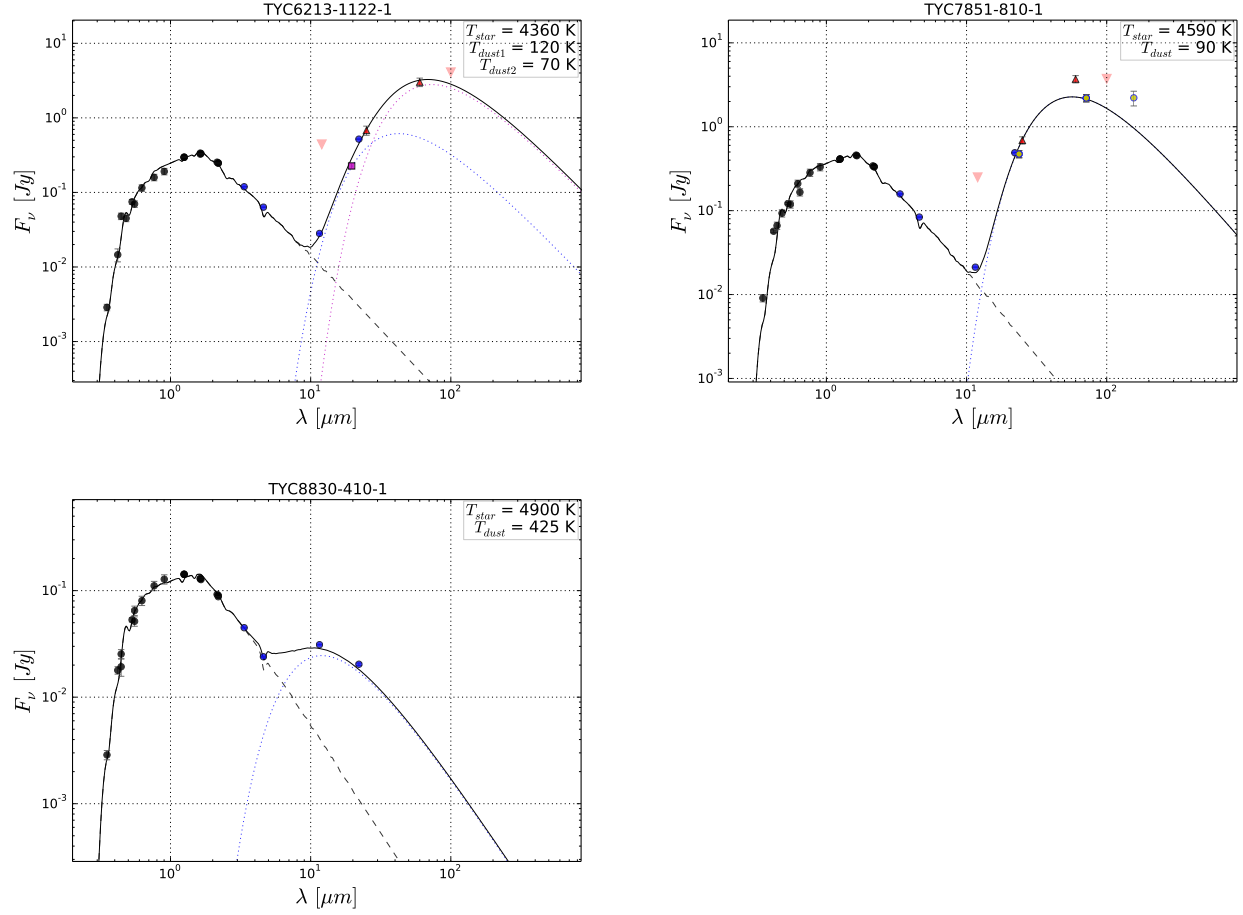


Fig. 13.— The newly discovered, dustiest disks in the Prime IR excess catalog. All of these targets display a fractional dust luminosity $> 10^{-2}$. The photometry plotted in each SED includes (not necessarily in every case) Johnson B, V (black circles), Tycho-2 B_T , V_T (black circles), *Sloan* g', r', i', z' (black circles), 2MASS J, H, K (black circles), WISE W1, W2, W3, and W4 (blue circles), Akari 9 and $18\mu m$ (magenta squares), MIPS 24 and $70\mu m$ (yellow circles), and IRAS 12, 25, 60 and $100\mu m$ (red triangles) from the optical to the far-IR. A description of each star can be found in Section 6.1.

TABLE 1
COMPLETED INFRARED SPACE MISSION INSTRUMENTS.

Instrument	Filter Wavelength (μm)	Ang Res (arcsec)	Yr of Launch	Comments
IRAS	12, 25, 60, 100	30 - 120	1983	all-sky, 96%, 250,000 sources
ISO	2.5 - 240	1.5 - 90	1995	30,000 pointed obs.
<i>Spitzer</i> MIPS	24, 70, 160	6 - 40	2003	~42 million pointed obs.
Akari	9, 18	~60	2006	all-sky, 870,000 sources
<i>Herschel</i> PACS	70, 100, 160	5 - 13	2008	~40,000 pointed obs.
<i>Herschel</i> SPIRE	250, 350, 500	18 - 36	2008	~40,000 pointed obs.
WISE	3.5, 4.6, 12, 22	6.1 - 12	2009	all-sky, >500 million sources
AllWISE	3.5, 4.6, 12, 22	6.1 - 12	2009	all-sky, >740 million sources

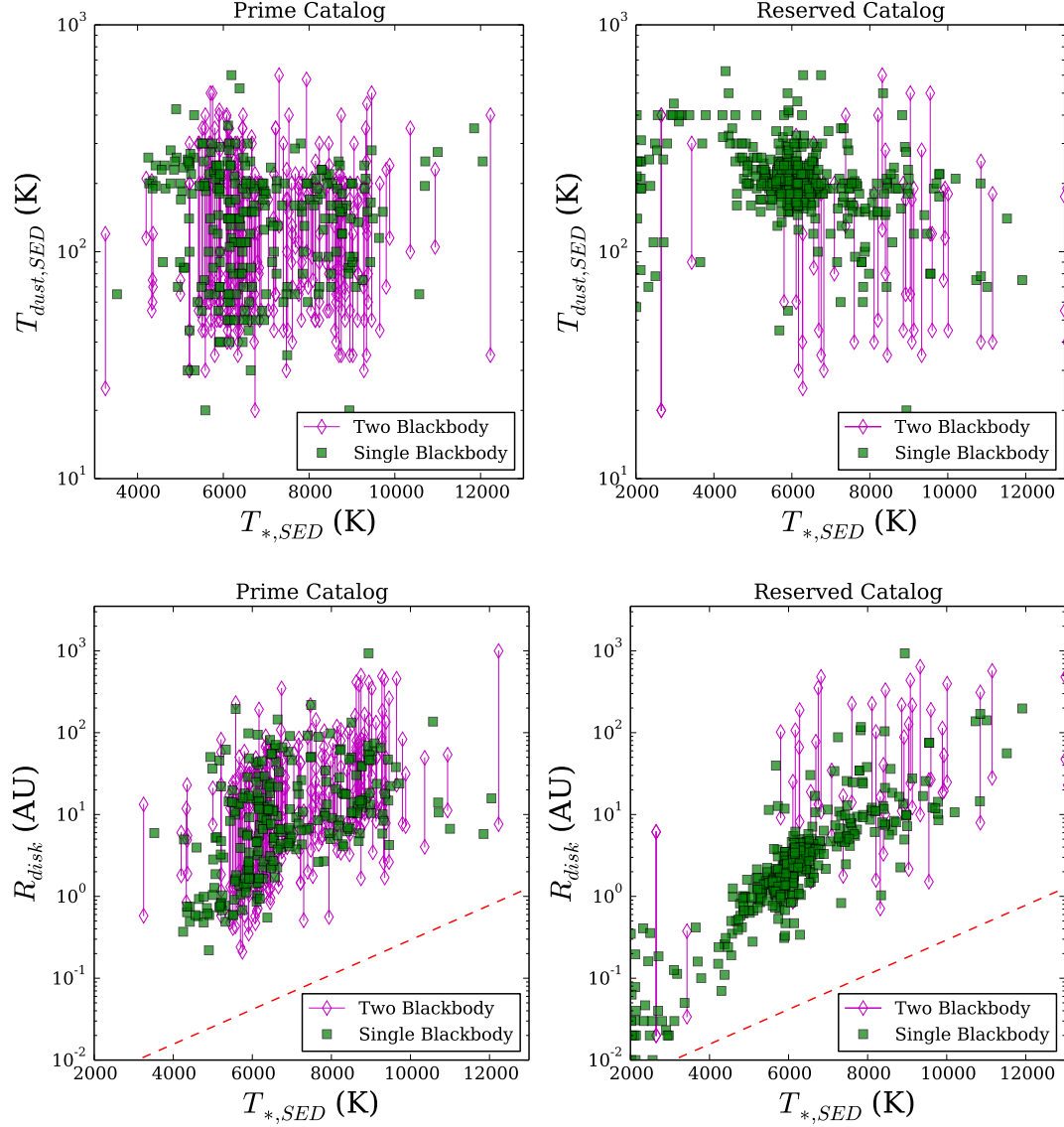


Fig. 14.— Top: Dust temperature for the range of spectral types included in the Prime IR excess catalog (*Left*; Table 3) and the Reserved IR excess catalog (*Right*; Table 4). The filled squares correspond to single blackbody dust fit. The unfilled diamonds are the IR excess stars that are best fit with two blackbody fits and the line connects the two. The sample of the Reserved catalog that is plotted display excess at more than one passband as without this criteria, the disk fitting procedure remains unconstrained.

Bottom: Disk radius in AU for the single and two blackbody fits compared the spectral type of the star using the best fit SED temperature for the Prime catalog (*Left*) and the Reserved catalog (*Right*). The dashed red line indicates the dust sublimation radius for silicate grains behaving as blackbodies at a sublimation temperature of 1500 K (Moro-Martin 2013).

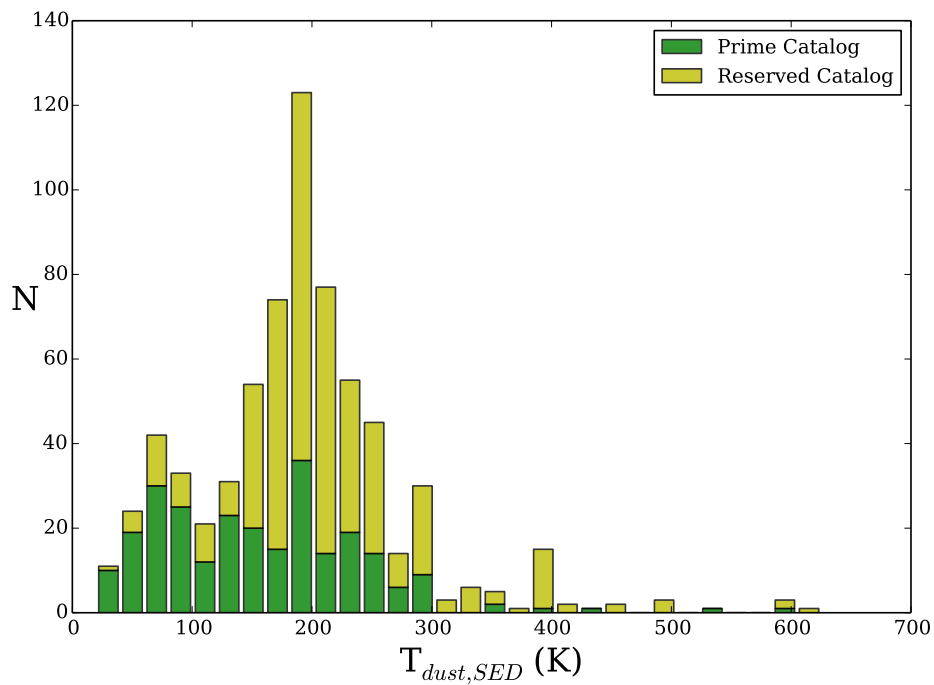


Fig. 15.— Distribution of dust temperatures for stars best fit using a single blackbody fit in the Prime and Reserved catalogs. Only stars with multiple passbands that display IR excess are included in this figure.

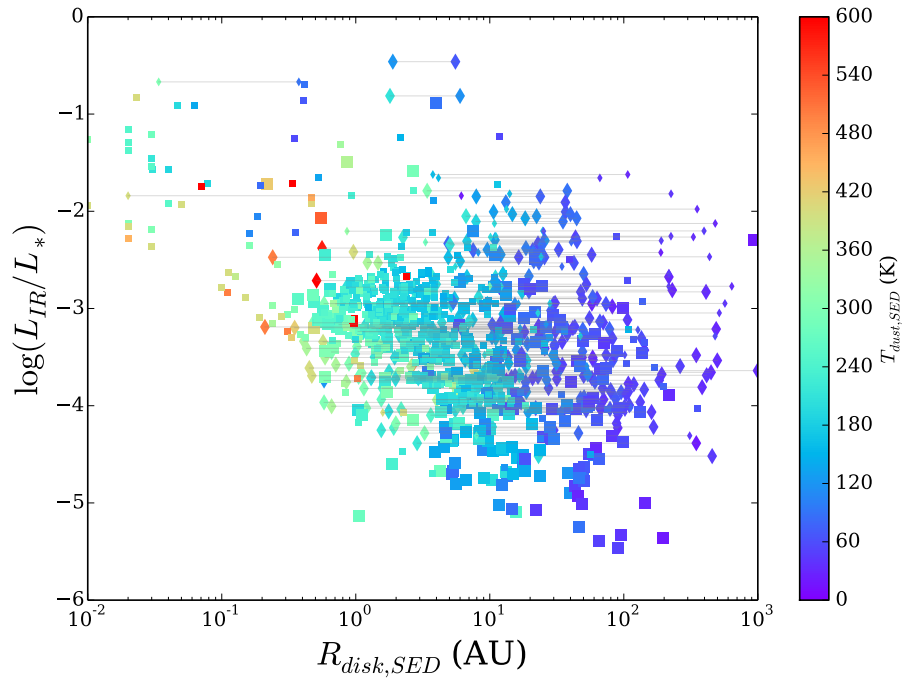


Fig. 16.— Disk radius in AU versus the fractional dust luminosity (τ) for the Prime (large symbols) and Reserved (small symbols) IR excess catalogs. The squares correspond to single blackbody dust fit. The diamonds are the stars that are best fit with two blackbody fits and the line connects the two. The color corresponds to the temperature of the dust.

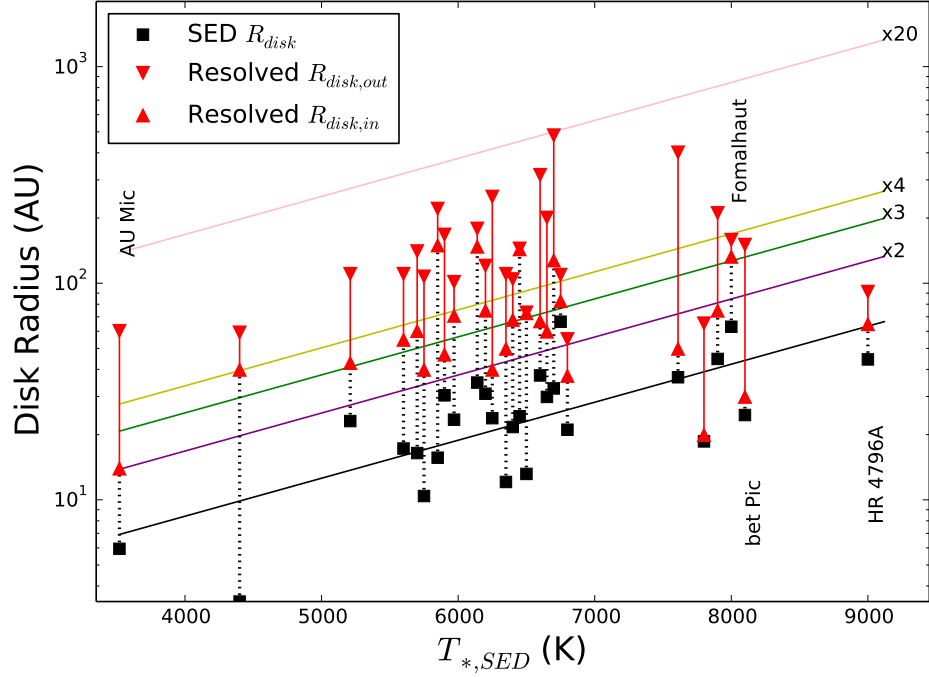


Fig. 17.— Comparison of the disk radius predicted by the SED blackbody model fit and the radius resolved through scattered light. The black squares are the SED disk radius in AU and the red triangles connected with the solid line are the extended dust range from inner to outer radius in AU. The names of some of the most well-known debris disks are shown. The unnamed stars are flagged in Tables 3 and 4. The solid black line indicates the fit to the SED disk radius (squares) and the consecutive lines indicate the amount of increase to that fit. The purple, green, yellow, and pink line shows twice, three times, four times, and 20 times the original fit, respectively.

TABLE 2

SUMMARY OF REFERENCES USED IN LITERATURE SEARCH FOR PREVIOUSLY CLAIMED IR EXCESS STARS.

Author	Year	Author	Year	Author	Year
Aumann et al.	1984	Sadakane & Nishida	1986	Jura	1991
Patten & Willson	1991	Oudmaijer et al.	1992	Mannings & Barlow	1998
Decin et al.	2000	Song et al.	2001	Spangler et al.	2001
Sylvester et al.	2001	Laureijs et al.	2002	Song et al.	2002
Weinberger et al.	2003	Wyatt et al.	2003	Gorlova et al.	2004
Greaves et al.	2004	Jura et al.	2004	Liu et al.	2004
Metchev et al.	2004	Zuckerman & Song	2004	Zuckerman et al.	2004
Beichman et al.	2005	Chen et al.	2005	Chen et al.	2005
Greaves et al.	2005	Kim et al.	2005	Low et al.	2005
Najita et al.	2005	Rieke et al.	2005	Song et al.	2005
Su et al.	2005	Beichman et al.	2006	Beichman et al.	2006
Bryden et al.	2006	Bryden et al.	2006	Carpenter et al.	2006
Chen et al.	2006	Gorlova et al.	2006	Goto et al.	2006
Hernandez et al.	2006	Hines et al.	2006	Kalas et al.	2006
Lestrade et al.	2006	Moor et al.	2006	Riaz et al.	2006
Silverstone et al.	2006	Smith et al.	2006	Su et al.	2006
Williams & Andrews	2006	Cieza et al.	2007	Gautier et al.	2007
Gorlova et al.	2007	Guieu et al.	2007	Hernandez et al.	2007
Kalas et al.	2007	Kalas et al.	2007	Lafreniere et al.	2007
Lisse et al.	2007	Luhman et al.	2007	Matthews et al.	2007
Matthews et al.	2007	Moerchen et al.	2007	Moerchen et al.	2007
Moro-Martin et al.	2007	Rhee et al.	2007	Rhee et al.	2007
Siegler et al.	2007	Trilling et al.	2007	Wyatt et al.	2007
Wyatt et al.	2007	Absil et al.	2008	Brown et al.	2008
Chen et al.	2008	Cieza et al.	2008	Gautier et al.	2008
Hernandez et al.	2008	Hillenbrand et al.	2008	Kastner et al.	2008
Marois et al.	2008	Merin et al.	2008	Meyer et al.	2008
Rebull et al.	2008	Rhee et al.	2008	Roberge & Weinberger	2008
Smith et al.	2008	Su et al.	2008	Trilling et al.	2008
Weinberger	2008	Wyatt	2008	Akeson et al.	2009
Balog et al.	2009	Booth et al.	2009	Brown et al.	2009
Bryden et al.	2009	Carpenter et al.	2009	Fujiwara et al.	2009
Fujiwara et al.	2009	Gaspar et al.	2009	Greaves et al.	2009
Gutermuth et al.	2009	Hernandez et al.	2009	Kospal et al.	2009
Lawler et al.	2009	Lestrade et al.	2009	Maness et al.	2009
Melis et al.	2009	Metchev et al.	2009	Moor et al.	2009
Morales et al.	2009	Nilsson et al.	2009	Plavchan et al.	2009
Roccatagliata et al.	2009	Schneider et al.	2009	Sicilia-Aguilar et al.	2009
Smith et al.	2009	Smith et al.	2009	Su et al.	2009
Tanner et al.	2009	Ardila et al.	2010	Bonsor et al.	2010
Buenzli et al.	2010	Cieza et al.	2010	Duchene	2010
Eiroa et al.	2010	Gizis	2010	Greaves et al.	2010
Grinin et al.	2010	Kastner et al.	2010	Kennedy et al.	2010
Koerner et al.	2010	Krivov et al.	2010	Lagrange et al.	2010
Liseau et al.	2010	Matthews et al.	2010	Melis et al.	2010
Moerchen et al.	2010	Monin et al.	2010	Moro-Martin et al.	2010
Nilsson et al.	2010	Rebull et al.	2010	Sierchio et al.	2010
Smith & Wyatt	2010	Stock et al.	2010	Thompson et al.	2010
Vandenbussche et al.	2010	Wahhaj et al.	2010	Chen et al.	2011
Churcher et al.	2011	Churcher et al.	2011	Currie et al.	2011
Desidera et al.	2011	Eiroa et al.	2011	Golimowski et al.	2011
Heng	2011	Kennedy et al.	2011	Marshall et al.	2011
Millan-Gabet et al.	2011	Moor et al.	2011	Morales et al.	2011
Patience et al.	2011	Peterson et al.	2011	Smith et al.	2011
Williams & Cieza	2011	Wilner et al.	2011	Zuckerman et al.	2011
Acke et al.	2012	Avenhaus et al.	2012	Chen et al.	2012
Cieza et al.	2012	Dahm et al.	2012	Donaldson et al.	2012
Ertel et al.	2012	Kennedy et al.	2012	Lawler & Gladman	2012

TABLE 2—*Continued*

Author	Year	Author	Year	Author	Year
Lebreton et al.	2012	Lestrade et al.	2012	Luhman & Mamajek	2012
Maldonado et al.	2012	Melis et al.	2012	Meng et al.	2012
Mizusawa et al.	2012	Morales et al.	2012	Riaz & Gizis	2012
Riviere-Marichalar et al.	2012	Riviere-Marichalar et al.	2012	Rodigas et al.	2012
Rodriguez & Zuckerman	2012	Schneider et al.	2012	Smith & Jeffries	2012
Urban et al.	2012	Wyatt et al.	2012	Zuckerman & Song	2012
Zuckerman et al.	2012	Ballering et al.	2013	Bonsor et al.	2013
Booth et al.	2013	Broekhoven-Fiene et al.	2013	Bulger et al.	2013
Eiroa et al.	2013	Fujiwara et al.	2013	Gaspar et al.	2013
Janson et al.	2013	Mathews et al.	2013	Melis et al.	2013
Moor et al.	2013	Morales et al.	2013	Olofsson et al.	2013
Panic et al.	2013	Riviere-Marichalar et al.	2013	Schneider et al.	2013
Thalmann et al.	2013	Wahhaj et al.	2013	Bailey et al.	2014
Ballering et al.	2014	Bonsor et al.	2014	Carpenter et al.	2014
Esplin et al.	2014	Greaves et al.	2014	Greaves et al.	2014
Kennedy et al.	2014	Kennedy et al.	2014	Liu et al.	2014
Marshall et al.	2014	Panic et al.	2014	Pawellek et al.	2014
Ricci et al.	2014	Riviere-Marichalar et al.	2014	Rodigas et al.	2014
Soummer et al.	2014	Thureau et al.	2014	Wittenmyer et al.	2014
Hung et al.	2015	Jang-Condell et al.	2015	Maldonado et al.	2015
Moor et al.	2015	Rodigas et al.	2015		

Table 3.: Prime IR Excess Stars from the Literature and Tycho-2 cross-correlation with ALLWISE

Name	R.A. & Dec	Spectral Type	T_{*SED} (K)	R_{*SED} (R_{\odot})	T_{dust} (K)	R_{disk} (AU)	T_{dust2} (K)	R_{disk2} (AU)	$\frac{L_{IR}}{L_{star}} (\times 10^{-4})$	Dist. (pc)	Num Excess	λ_{start} (μm)	Has IRS?	Known Reference
HR 9102	00:04:20.3 -29:16:07	A0V	8820	2.58	200	11.6	70	95.5	1.37	124.84	2	22	N	Su et al. 2006
HD 105	00:05:52.6 -41:45:11	G0V	6070	1.01	390	0.5	50	34.6	4.53	39.38	3	22	Y	Zuckerman & Song 2004a
HD 166	00:06:37.1 +29:01:15	K0V	5700	0.78	300	0.6	70	12.1	3.56	13.67	4	22	Y	Bryden et al. 2006b
HD 203	00:06:50.1 -23:06:27	F3V	6710	1.48	160	6.0	-	-	1.69	39.38	3	22	Y	Rebull et al. 2008
HD 377 ^b	00:08:25.8 +06:37:00	G2V	5910	1.03	200	2.1	60	23.4	5.31	39.07	3	22	Y	Moor et al. 2006
sig And	00:18:19.6 +36:47:06	A2V	8780	2.00	155	14.9	-	-	0.19	41.32	3	22	Y	Morales et al. 2009
HD 1466	00:18:26.2 -63:28:39	F8V	6140	1.06	140	4.7	-	-	1.68	41.54	2	22	Y	Smith et al. 2006
HD 1461	00:18:42.1 -08:03:12	G3V	5880	1.07	65	20.5	-	-	0.50	23.24	1	22	Y	Lawler et al. 2009
9 Cet	00:22:51.7 -12:12:33	G3V	5920	0.95	40	48.5	-	-	0.09	20.86	2	60	Y	Chen et al. 2014
kap Phe	00:26:12.3 -43:40:46	A5IVn	8010	1.76	170	9.0	-	-	0.18	23.80	3	22	Y	Rieke et al. 2005
HD 2834	00:31:24.9 -48:48:12	A1Va	8950	2.24	95	46.3	-	-	0.17	52.96	1	22	Y	Chen et al. 2014
HD 2772	00:31:46.3 +54:31:20	B8Vn	12230	3.50	400	7.6	35	995.0	2.29	115.74	4	11	N	Chen et al. 2005a
bet03 Tuc	00:32:44.0 -63:01:53	A0V	9050	1.63	300	3.4	150	13.8	2.73	45.55	5	11	Y	Song et al. 2001
HD 3126	00:34:27.1 -06:30:14	F4V	6380	1.23	200	2.9	45	57.8	1.91	40.91	1	22	Y	Trilling et al. 2008
HD 3296	00:36:02.0 -05:34:15	F5V	6450	1.46	60	39.2	-	-	0.23	45.04	1	22	Y	Trilling et al. 2008
HD 3670	00:38:56.7 -52:32:03	F5V	6440	1.35	290	1.5	55	43.1	6.47	83.12 ^a	1	22	Y	Moor et al. 2011
64 Psc	00:48:58.7 +16:56:26	F8V	6570	1.52	300	1.7	-	-	1.38	23.45	2	60	N	Koerner et al. 2010
HD 5133	00:53:01.1 -30:21:24	K2.5V	5170	0.66	30	45.7	-	-	0.11	14.17	3	60	N	Lawler et al. 2009
66 Psc	00:54:35.2 +19:11:18	A1Vn	9340	2.70	250	8.7	35	447.8	2.20	108.10	2	22	Y	Rhee et al. 2007
TYC2278-834-1	01:04:25.3 +31:18:27	K0	5310	0.78	260	0.7	-	-	6.19	62.89 ^a	2	11	N	-
V443 And	01:10:41.9 +42:55:54	G7V	5660	0.78	200	1.4	50	23.3	1.96	27.07	1	22	Y	Kim et al. 2005
HR 333	01:12:17.3 +79:40:26	A3V	8920	2.41	80	69.7	-	-	1.88	82.84	2	22	N	Jura et al. 2004
HD 7570	01:15:11.1 -45:31:54	F9VFe	6170	1.19	85	14.5	-	-	0.08	15.11	2	22	Y	Beichman et al. 2006a
HD 7590	01:16:29.1 +42:56:21	G0V	6090	0.90	200	1.9	40	48.8	3.13	23.19	1	22	Y	Plavchan et al. 2009
2MASS														
J01203226-1128035	01:20:32.3 -11:28:05	G9V	5500	0.75	300	0.5	-	-	1.96	34.39	1	22	Y	Carpenter et al. 2009
HD 8907	01:28:34.4 +42:16:02	F7	6250	1.23	50	45.0	-	-	2.85	34.77	1	22	Y	Zuckerman & Song 2004a
EO Psc	01:29:04.9 +21:43:23	K2.5V	4930	0.96	70	11.1	-	-	0.44	23.73	1	22	Y	Ballering et al. 2013
49 Cet	01:34:37.8 -15:40:34	A1V	8670	1.77	180	9.6	65	73.6	11.14	59.38	8	22	Y	Oudmaijer et al. 1992
EX Cet	01:37:35.5 -06:45:38	G5V	5440	0.75	200	1.3	60	14.5	1.95	23.95	2	22	Y	Plavchan et al. 2009
HD 10472	01:40:24.1 -60:59:56	F2IV/V	6610	1.34	200	3.4	60	37.9	5.47	67.24	2	22	Y	Zuckerman & Song 2004a
HD 10647 ^b	01:42:29.5 -53:44:27	F9V	6280	1.01	300	1.0	55	30.9	5.80	17.43	7	22	Y	Zuckerman & Song 2004a

Only a portion of this table has been shown here. Full content of this table is available in the online material.

Notes: The spectral types are taken from SIMBAD unless designated by a ‘:’. The Num.Excess parameter describes the number of passbands that demonstrate IR excess. The λ_{start} column offers an approximate starting wavelength for the IR excess. The IRS column designates whether this study was able to acquire IRS spectra from the Enhanced Products Archive which in many cases supplements the IR excess we report.

Footnotes:

^a : This flag indicates the distance shown is from the SED as described in detail in the text (Section 3.2.6).

^b : This flag indicates that the disk has been resolved through scattered light and plotted in Figure 18.

Table 4:: Reserved IR Excess Stars from the Literature and Tycho-2 cross-correlation with ALLWISE

Name	R.A. & Dec	Spectral Type	$T_{*,SED}$ (K)	$R_{*,SED}$ (R_{\odot})	T_{dust} (K)	R_{disk} (AU)	T_{dust2} (K)	R_{disk2} (AU)	$\frac{L_{IR}}{L_{star}}$ ($\times 10^{-4}$)	Dist. (pc)	Num Excess	λ_{start} (μm)	Has IRS?	Known Reference
TYC3660-183-1	00:00:11.5 +57:52:20	:A8	7130	1.470	150	7.70	-	-	0.910	132.41 ^a	1	22	N	-
TYC4026-379-1	00:01:18.6 +66:50:12	:F4	6540	1.350	260	1.90	-	-	3.100	116.38 ^a	2	11	N	-
TYC2789-507-1	00:03:08.3 +42:44:52	:A2	8430	3.080	70	103.90	-	-	2.690	162.33	2	22	N	-
TYC4294-584-1	00:05:20.0 +68:53:04	:A1	9130	2.410	140	23.80	-	-	0.490	169.49	1	22	N	-
TYC4667-1078-1	00:11:34.8 -03:04:38	:F8	6240	1.130	180	3.10	-	-	2.660	101.46 ^a	1	22	N	-
HD 870	00:12:50.0 -57:54:45	K0V	5550	0.750	300	0.60	45	26.630	1.570	20.18	1	60	Y	Lawler et al. 2009
TYC4026-208-1	00:13:03.4 +67:14:46	:K1	5190	0.760	170	1.60	-	-	17.270	184.32 ^a	2	11	N	-
HD 987	00:13:53.2 -74:41:18	G8V	5670	0.780	125	3.70	-	-	0.830	44.40	1	22	N	Zuckerman et al. 2011
HD 1237	00:16:12.6 -79:51:04	G8V	5650	0.820	300	0.60	-	-	1.630	17.49	1	60	Y	Beichman et al. 2005
TYC2272-1059-1	00:16:42.9 +36:37:47	:A2	8300	2.110	140	17.20	-	-	0.610	126.41	1	22	N	-
39 Psc	00:17:50.1 +16:19:51	F6V	6400	1.180	200	2.80	-	-	0.320	44.82	1	22	N	Mizusawa et al. 2012
26 And	00:18:42.1 +43:47:27	B8V	10850	3.760	75	169.30	-	-	2.450	202.83	2	22	N	Wyatt 2007
HD 1562	00:20:00.2 +38:13:35	G1V	5910	0.930	75	13.40	-	-	0.580	24.79	1	60	N	Koerner et al. 2010
TYC4015-1052-1	00:20:53.9 +61:27:42	:K6	4320	0.600	120	1.80	-	-	5.160	32.11 ^a	1	22	N	-
TYC8846-897-1	00:21:33.4 -66:18:16	A0V	9330	1.720	120	24.20	-	-	0.500	142.86	1	22	N	-
TYC4019-3245-1	00:22:05.1 +62:13:13	:K4	4850	0.690	165	1.30	-	-	8.240	93.56 ^a	1	22	N	-
TYC1186-730-1	00:23:11.9 +20:05:09	:A8	7190	1.230	140	7.50	-	-	1.090	105.26	1	22	N	-
TYC9135-268-1	00:34:53.4 -68:35:48	A0V	6940	2.230	340	2.10	-	-	2.300	182.81	2	11	N	-
TYC16-83-1 ^c	00:37:19.2 +07:29:10	:M	2830	0.130	300	0.03	-	-	47.830	1.75 ^a	1	22	N	-
eta Phe	00:43:21.1 -57:27:47	A0IV	9080	3.760	65	170.80	-	-	0.010	75.52	1	60	N	Su et al. 2006
HR 189	00:44:26.1 +47:51:50	B5V	13000	3.690	175	47.40	55	480.070	5.190	191.20	4	11	N	Chen et al. 2014
TYC3667-527-1	00:50:59.5 +59:41:35	:F5	6470	1.300	180	3.90	-	-	2.280	165.10 ^a	1	22	N	-
TYC8034-360-1	00:51:58.7 -49:47:04	:G2	5900	0.960	290	0.90	-	-	7.680	170.27 ^a	2	11	N	-
TYC4017-1710-1	00:53:28.1 +60:39:56	A0V	8250	3.030	140	24.40	-	-	0.690	253.16	1	22	N	-
HD 5349	00:55:11.7 -16:58:17	K0IV	5170	1.600	250	1.60	-	-	1.180	48.94	1	22	Y	Chen et al. 2014
TYC2802-1387-1	00:59:26.2 +40:09:18	:A3	7950	1.580	150	10.30	-	-	0.550	110.37	1	22	N	-
TYC3680-352-1	01:03:48.4 +58:09:36	:A3	8300	1.580	160	9.90	-	-	1.130	186.47 ^a	1	22	N	-
HD 6434	01:04:40.1 -39:29:17	G2/3V	5920	1.090	120	6.10	-	-	0.080	41.37	1	60	Y	Reid et al. 2007
TYC4021-1605-1	01:05:13.8 +62:25:26	:K6	4340	0.610	150	1.10	-	-	4.240	36.90 ^a	1	22	N	-
TYC25-152-1	01:05:38.5 +06:38:50	:G2	5890	0.960	180	2.40	-	-	60.130	259.96 ^a	2	11	N	-
TYC4021-680-1	01:07:35.5 +63:21:11	:G5	5660	0.880	300	0.70	-	-	4.340	71.15 ^a	2	11	N	-

Only a portion of the table has been shown here. Full table available in online materials.

Notes: The spectral types are taken from SIMBAD unless designated by a ':'. The Num.Excess parameter describes the number of passbands that demonstrate IR excess. The λ_{start} column offers an approximate starting wavelength for the IR excess. The IRS column designates whether this study was able to acquire IRS spectra from the Enhanced Products Archive which in many cases supplements the IR excess we report.

Footnotes:

^a : This flag indicates the distance shown is from the SED as described in detail in the text (Section 3.2.6).

^b : This flag indicates that the disk has been resolved through scattered light and plotted in Figure 18.

^c : This star is most likely a giant based on the difference between proper motion magnitude and SED distance. Needs spectroscopic confirmation.

TABLE 5

PHOTOMETRY INFORMATION FOR PRIME AND RESERVED CATALOG STARS.

Column	Explanation
1	Source identifier
2-8	RA/DE (J2000)
9	Catalog Membership
10	SED Effective Temperature
11	Stellar Radius (R_{\odot})
12-14	W1 measurement (Jy), Uncertainty, Predicted photospheric measurement
15-17	W2 measurement (Jy), Uncertainty, Predicted photospheric measurement
18-20	W3 measurement (Jy), Uncertainty, Predicted photospheric measurement
21-23	W4 measurement (Jy), Uncertainty, Predicted photospheric measurement
24-26	IRAS $12\mu\text{m}$ measurement (Jy), Uncertainty, Predicted photospheric measurement
27-29	IRAS $25\mu\text{m}$ measurement (Jy), Uncertainty, Predicted photospheric measurement
30-32	IRAS $60\mu\text{m}$ measurement (Jy), Uncertainty, Predicted photospheric measurement
33-35	IRAS $100\mu\text{m}$ measurement (Jy), Uncertainty, Predicted photospheric measurement
36-39	MIPS $24\mu\text{m}$ measurement (Jy), Uncertainty, Reference, Predicted photospheric measurement
40-43	MIPS $70\mu\text{m}$ measurement (Jy), Uncertainty, Reference, Predicted photospheric measurement
44-47	MIPS $160\mu\text{m}$ measurement (Jy), Uncertainty, Reference, Predicted photospheric measurement
48-51	PACS $70\mu\text{m}$ measurement (Jy), Uncertainty, Reference, Predicted photospheric measurement
52-55	PACS $100\mu\text{m}$ measurement (Jy), Uncertainty, Reference, Predicted photospheric measurement
56-59	PACS $160\mu\text{m}$ measurement (Jy), Uncertainty, Reference, Predicted photospheric measurement
60-63	SPIRE $250\mu\text{m}$ measurement (Jy), Uncertainty, Reference, Predicted photospheric measurement
64-67	SPIRE $350\mu\text{m}$ measurement (Jy), Uncertainty, Reference, Predicted photospheric measurement
68-71	SPIRE $500\mu\text{m}$ measurement (Jy), Uncertainty, Reference, Predicted photospheric measurement

Table 5 is published in its entirety in the electronic edition
of the *Astrophysical Journal*. A portion is shown here
for guidance regarding its form and content.